REPORT DOCUMENTATION PAGE

Form Approved
OMB No. 0704-0188

1. REPORT DATE (DD-MM-YYYY)	2. REPORT TYPE	3. DATES COVERED (From – To)
	Final Technical Report	1April 2003 – 30 September 2006

4. TITLE AND SUBTITLE
Multifunctional Polymers and Composites for Self-Healing Applications

5a. CONTRACT NUMBER

5b. GRANT NUMBER
F49620-03-1-0179

5c. PROGRAM ELEMENT NUMBER

6. AUTHOR(S)
Scott R. White

5d. PROJECT NUMBER

5e. TASK NUMBER

5f. WORK UNIT NUMBER

7. PERFORMING ORGANIZATION NAME(S) AND ADDRESS(ES
University of Illinois at Urbana-Champaign
306 Talbot Lab
104 S. Wright Street
Urbana IL 61801

8. PERFORMING ORGANIZATION REPORT NUMBER

9. SPONSORING/MONITORING AGENCY NAME(S) AND ADDRESS(ES)
Air Force Office of Scientific Research (AFOSR)
875 N. Arlington St., Rm. 3112
Arlington, VA 22203
Dr Byung Lip Lee/NA

10. SPONSOR/MONITOR'S ACRONYM(S)
AFOSR

11. SPONSORING/MONITORING AGENCY REPORT NUMBER
AFRL-SR-AR-TR-07-0224

12. DISTRIBUTION AVAILABILITY STATEMENT
DISTRIBUTION A: Approved for public release. Distribution is unlimited.

13. SUPPLEMENTARY NOTES

14. ABSTRACT
Mechanical deformation can be used to activate specific reaction pathways in mechanochemical triggers designed to harness the energy in a polymer under stress. Since activation of these triggers occurs before chain scission, we feel that they will be useful for the development of self-toughening polymeric materials. Upon activation, the oQDM intermediates could react with pendant dienophiles to form new crosslinks. The formation of crosslinks would be directly coupled and tailored to the stress field in a failing polymer. We also feel, with slight modification, that mechanochemical triggers could be useful for the stress-induced formation of new chromophores. The newly formed chromophores could then signal that some critical load has been reached, or perhaps signal the presence of microcracks. We expect that the procedures reported here will be generally useful for the development of utilizing mechanical energy to activate specific chemical pathways, and help shift the major focus of mechanochemical studies from bond-breaking to bond-making transformations.

15. SUBJECT TERMS

16. SECURITY CLASSIFICATION OF:			17. LIMITATION OF ABSTRACT	18. NUMBER OF PAGES	19a. NAME OF RESPONSIBLE PERSON
a. REPORT	b. ABSTRACT	c. THIS PAGE	Unclassified	61	19b. TELEPONE NUMBER (*Include area code*)
Unclassified	Unclassified	Unclassified			(703)

Multifunctional Polymers and Composites for Self-Healing Applications

FINAL TECHNICAL REPORT

AFOSR GRANT # F49620-03-1-0179

4/1/2003-9/30/2006

Scott R. White (PI), Jeffrey S. Moore (co-PI), Nancy R. Sottos (co-PI)
swhite@uiuc.edu, jsmoore@uiuc.edu, n-sottos@uiuc.edu

University of Illinois at Urbana-Champaign
306 Talbot Lab, 104 S. Wright St.
Urbana, IL 61801

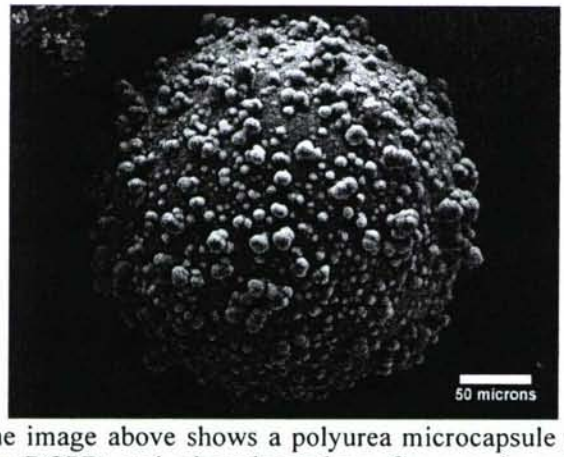

The image above shows a polyurea microcapsule of exo-DCPD and phenylacetylene for use in self-healing epoxy catalyzed by Tungsten hexachloride, a new and cost-effective healing system. [Photo: J. Kamphaus, Univ. of Illinois, 2006]

OBJECTIVES

The objectives of this research project was to develop multifunctional self-healing polymers and composite materials appropriate for DOD and Air Force applications. A multidisciplinary basic research program was carried out with the following technical tasks:

- screen a broad spectrum of potential matrix/healing agent systems using chemical and mechanical compatibility protocols,
- optimize ring-opening-metathesis-polymerization (ROMP) chemistry for self-healing applications,
- explore new healing chemistries utilizing ring-opening polymerization of cyclic ester and carbonate monomers and other copolymerization strategies,
- develop new mechanochemical triggering concepts for self-healing polymers.

STATUS

This project began 4/1/03 and concluded on 9/30/06. A new healing chemistry was developed and the initial demonstration of a new healing concept using mechanochemical triggers was demonstrated. The main results of these activities are summarized below.

RESULTS

1. A New Self-healing Epoxy with Tungsten (VI) Chloride Catalyst

Self-healing materials are inspired by many biological examples in which the healing process is triggered, regulated, and completed in an autonomic fashion. For structural applications the healing of bone (Fratzl 2007) serves as a rich source of concepts for functional adaptation in response to damage and stress state. How these concepts are being integrated in synthetic materials was also the subject of a recent special issue on the topic (Sottos *et al.* 2007).

Several techniques for achieving self-healing functionality in polymer materials have been demonstrated. These approaches include the incorporation of microcapsules (White *et al.* 2001) or hollow glass fibers containing healing agent (Pang and Bond 2005), the use of a microvascular network to deliver healing agent throughout a structure (Toohey *et al.* 2007), utilizing reversible cross-linking to induce mending after heating via molecular linkages (Chen *et al.* 2002), and a phase separated system based on polydimethylsiloxane (Cho *et al.* 2006). Self-healing occurs when monomer is released and initiated by an embedded catalyst phase (Toohey *et al.* 2007; White *et al.* 2001) or when a two-part resin system is released simultaneously in the crack plane (Pang and Bond 2005). Healing efficiencies of over 90 % have been achieved for *in situ* samples with a healing chemistry that uses benzylidene-bis(tricyclohexylphosphine) dichlororuthenium (Grubbs' catalyst) to initiate ring opening metathesis polymerization (ROMP) of the *endo* isomer of dicyclopentadiene (DCPD) (Brown *et al.* 2002). Mauldin and co-workers (2007) explored ROMP using the *exo* isomer of DCPD and Grubbs' catalyst and found that healing

reached steady state ca. twenty times faster compared to *endo*-DCPD, but at the expense of a maximum achievable healing efficiency (ca. 60 % of that reached for the *endo*-DCPD). Although Grubbs' catalyst has a nearly ideal chemical selectivity, its high cost, restricted availability and limited temperature stability preclude its use in high volume, commercial composite and polymeric parts.

Alternative catalyst precursors for ROMP healing have been surveyed (Rule 2005) and tungsten (VI) chloride (WCl_6) with a co-activator were identified to have the greatest potential to address many of the limitations previously indicated. WCl_6 is a cost-effective alternative that is widely available and has a melting point of T_m = 275 °C, which is significantly higher than that of Grubbs' catalyst (T_m = 153 °C). The commercial potential of this class of tungsten catalyst systems has been demonstrated in the Metton® (Metton America, Inc.) liquid molding two part resin system based on the ROMP of *endo*-DCPD (Breslow 1990).

In catalyst systems based on WCl_6, the WCl_6 itself is not the active catalyst, but rather a catalyst precursor. A key step in forming an active catalyst is the alkylation of the tungsten, and this is usually accomplished by the addition of a separate co-activator. In controlled environments (i.e. no air or impurities are present), the most effective co-activators are aggressive alkylating agents such as organoaluminum compounds (Breslow 1990), but they are also extremely sensitive to air and other impurities. This sensitivity makes them inappropriate for self-healing in an air environment. Therefore, as a more stable alkylating agent, we chose to use phenylacetylene, which has been shown to be an effective co-activator with WCl_6 even in air (Katz and Han 1982). In formulating this self-healing system, we also include nonylphenol as a dissolution agent (Breslow 1990). This component is necessary because self-healing is triggered by the dissolution of the catalyst into the healing agent (DCPD), and without nonylphenol, WCl_6 is nearly insoluble in DCPD.

It is also worth noting that the air environment of the self-healing reaction is expected to affect the WCl_6. A likely initial oxidation product is $WOCl_4$, which is also a ROMP-active catalyst (Balcar *et al.* 1992). Furthermore, $WOCl_4$ has been claimed to be a necessary component (in addition to the WCl_6) for effective catalysis (Breslow 1990). Therefore, for the purpose of this work, we consider both WCl_6 and any $WOCl_4$ generated by oxidation to be active catalyst precursors.

We report on the viability of WCl_6 as a ROMP active catalyst precursor for self-healing polymers. Environmental stability of this catalyst precursor was evaluated using ultraviolet-visible (UV-vis) absorbance spectrophotometry with three different WCl_6 delivery methods. The healing performance associated with each delivery method was evaluated by fracture experiments. The use of a coupling agent to increase the virgin (initial) fracture toughness was explored, as well as the effect of WCl_6 dispersion and concentration on healing performance.

1.1 Materials and Methods

a) WCl_6 Delivery Methods

WCl_6 is sensitive to both moisture and the processing environment of curing epoxy resins (Rule 2005). In addition to as-received WCl_6 (Aldrich), recrystallized, and a wax-protected form of WCl_6 were prepared for use in self-healing epoxy. The morphology of as-received WCl_6 is shown in Figure 1.1a. The average particle sizes determined by analysis of SEM images for all three delivery methods are listed in Table 1.1.

The recrystallized and wax-protected WCl_6 were prepared in a nitrogen-filled glove box or using standard Schlenk techniques (Shriver and Drezdzon 1986). Recrystallized WCl_6 was prepared according to the procedure outlined by Ketellaar and Van Oosterhout (1943). WCl_6 (18.0 g) was placed in a sealed heavy-walled flask with 200 mL of dry CCl_4 (Aldrich) and heated to 120 °C in an oil bath. After 30 min, heating was stopped, and the sample was left to cool slowly. The resulting mixture was filtered, and the WCl_6 particles were dried under vacuum. The product was then sieved and particles smaller than 180 μm were used for chemical and mechanical testing. Recrystallized WCl_6 morphology (Figure 1.1b) shows a high aspect ratio planar geometry, in contrast to the as-received form. The crystal structures of both the as-received and recrystallized WCl_6 were confirmed by X-ray diffraction to be the hexagonal α-WCl_6 polymorph (Ketelaar and van Oosterhout 1943).

A third delivery method was investigated in which the as-received WCl_6 was dissolved and dispersed in a paraffin wax bead in order to provide protection from potential deactivation by amines during curing of the epoxy matrix. A similar protection scheme was used by Rule and co-workers (2005) for Grubbs' catalyst. WCl_6 (5.25 g) was added to a 40 mL vial with 730 mg of the dissolution agent nonylphenol (Aldrich) and 9.0 g of paraffin wax (melting point of 58-62 °C, Aldrich). The dissolution agent was added to compatibilize the WCl_6 with the wax beads and to facilitate dissolution in the DCPD healing agent. The vial was capped and placed in a 120 °C bath and magnetically stirred. In a separate bath, 300 mL of dry perfluorodecalin (Flutec PP6, F2 Chemicals) was stirred at 1250 rpm with a mechanical mixer in a 1000 mL beaker until it reached a temperature of 65 °C. Upon complete melting of the wax, the sample mixture was poured into the perfluorodecalin bath and allowed to stir for one minute. Approximately 700 mL of chilled perfluorodecalin was quickly added to the hot perfluorodeclin bath to quench the suspension and solidify the wax beads. The perfluorodecalin and wax mixture was vacuum filtered and the wax beads (Figure 1.1c) were dried under vacuum. The beads were then sieved and the beads smaller than 355 μm were kept for further study. Elemental analysis of the wax beads revealed that the concentration of tungsten was 10 wt% while the theoretical tungsten concentration based on the mixture ratio was 16%. After processing, a dense solid remained in the vial suggesting incomplete dissolution of the WCl_6 had occurred.

b) Assessment of Environmental Stability

Environmental stability of the three forms of WCl_6 was monitored using ultraviolet-visible absorbance spectrophotometry. Samples exposed to air (22 °C, 30 % relative humidity) for 0, 2 or 24 hours were brought into an argon filled glove box and dissolved in dry toluene at a concentration of 0.8 mM of tungsten. The UV-vis absorbance spectra were taken at wavelengths from 280-800 nm in quartz cuvettes (path length of 0.1 cm) with Teflon seals.

c) Sample Preparation

Tapered double-cantilever beam (TDCB) fracture specimens (Brown *et al.* 2002) were adopted to evaluate healing performance. The tapered geometry allows for a crack length independent fracture toughness measurement. Localized TDCB specimens, as shown in Figure 1.2, were manufactured using Epon® 828 epoxy resin (Miller-Stephenson) cured with 12 pph Ancamine® DETA (Air Products). Because the crack is directed along the centerline of the specimens, only the material near the centerline is utilized during self-healing. Therefore, the sample was made in two stages such that only the material near the centerline possesses self-healing functionality. A method developed by Rule and co-workers (2007) was used in which a non self-healing blank was formed in the outer regions of the TDCB geometry by pouring neat resin epoxy into a silicon rubber mold that contained a 7 mm wide insert around the grooved section of the sample. The blanks used

for *in-situ* samples also contained microcapsules at the same concentration as the center material. Rule and co-workers (2007) found that the measured fracture toughness was artificially high for *in situ* samples with no capsules in the blank. However, by incorporating the same concentration of microcapsules in the blank the modulus and thermal expansion coefficient are matched with the self-healing center and accurate fracture toughness data are obtained. The blank was then cured for 24 hours at 22 °C.

The insert was subsequently removed and the self-healing material was prepared for the second stage of specimen manufacturing. Two types of samples were fabricated: self activated and *in-situ*. Self-activated samples contained WCl_6 but no healing agent and in-situ samples contained both WCl_6 and microencapsulated DCPD (Brown *et al.* 2002). Epoxy resin was degassed and allowed to react for 30 minutes prior to the addition of WCl_6 to permit time for the viscosity of the resin to increase (preventing settling of WCl_6 particles) and reduce the concentration of free amines. The desired amount of WCl_6 was then added to the epoxy resin. Higher concentrations of wax-encapsulated WCl_6 (>20 wt%) were not possible due to excessive viscosity of the resin mixture. Unless otherwise stated, samples were mixed by hand. The effect of WCl_6 dispersion was investigated by comparing hand mixed and mechanically mixed samples.

For *in-situ* self-healing samples, microcapsules were also added to the mixture at this time. These microcapsules contained *exo*-DCPD, phenylacetylene (45 mM), and nonylphenol (45 mM) and were manufactured by an established interfacial polymerization encapsulation technique (Brown *et al.* 2003). The resulting capsules were sieved and the distribution used for analysis was 188 ± 31 μm. The resin mixture was then poured into the center of the blank and the mold was closed. All samples were cured for 24 hours at 22 °C followed by an additional 24 hours at 35 °C. The samples were removed from the molds, allowed to cool to 22 °C, and then tested.

d) Mechanical Assessment of Healing Performance

TDCB fracture specimens were similar to those used by Rule and co-workers (2007), but with a nominal crack width of 3.8 mm and an overall specimen thickness of 7.1 mm. The fracture toughness is determined as

$$K_{Ic} = \alpha P_c \tag{1.1}$$

where P_c is the critical fracture load and α is a scaling parameter that depends on the specimen geometry and material properties and is equal to 8,777 $m^{-3/2}$ which was calculated from Brown and co-workers data (2002) for the thicker samples used here. The healing efficiency was calculated as

$$\eta = \frac{K_{Ic}^{healed}}{K_{Ic}^{virgin}} = \frac{P_c^{healed}}{P_c^{virgin}} \tag{1.2}$$

where P_c^{virgin} is the critical fracture load of the initial fracture and P_c^{healed} is the critical fracture load after healing.

Some samples exhibited a non-linear response after healing. These experiments were analyzed using a method outlined by Rule and co-workers (2005) which defines an alternative healing efficiency as

$$\eta' = \frac{A_{healed} \Big/ b_n\left(W - a_o^{healed}\right)}{A_{virgin} \Big/ b_n\left(W - a_o^{virgin}\right)} \tag{1.3}$$

where A is the total area under the load-displacement curve, b_n is the width of the crack plane (3.8 mm), W is the distance from the center of the loading pins to the end of the specimen (79.3 mm), a_o^{virgin} is the initial crack length for the virgin test, and a_o^{healed} is the initial crack length for the healed test. Both η (the recovery of the linear-elastic fracture toughness) and η' (the recovery of the total fracture energy) are independent measures of healing efficiency and they cannot be directly compared.

The testing of the TDCB samples followed previously established protocols for self-activated samples where the samples contain the catalyst phase and the healing agent is manually injected into the crack (Brown *et al.* 2002). A small starter crack was initiated by tapping a razor blade into a molded starter notch. The samples were pin loaded in Mode I using displacement control at 5 μm/s until complete failure. After the virgin (initial) test the two pieces of the sample were brought back together in alignment while maintaining a small gap of approximately 1 mm between the crack faces. Approximately 100 μL of a healing solution was then injected between the crack faces. For samples containing wax-protected WCl_6, the healing solution was prepared by mixing 5 μL of phenylacetylene (Aldrich) and 1 mL of *exo*-DCPD synthesized from *endo*-DCPD (Acros) (Nelson and Kuo 1975). For samples containing as-received or recrystallized WCl_6, 10 mg of nonylphenol, a dissolution agent, was added to the above-mentioned healing solution. The nonylphenol was omitted from the healing solution for wax-protected WCl_6, as it is already present in the wax beads. Once the healing solution was injected, the crack faces were then brought into full contact and left undisturbed for 48 hours. After healing, the samples were tested again without initiating another starter crack. Figures 1.3a, 1.3c and 1.3d contain typical load vs. displacement plots for self-activated recrystallized, as-received, and wax encapsulated delivery methods. For the as-received and recrystallized samples, a two stage failure process was observed. Healed specimens exhibited an initial linear elastic response until reaching a critical fracture load after which a precipitous drop in load-carrying capability was observed. Continued deformation of the samples leads to a lengthy and gradual decline in load and a ductile-type failure mode that absorbs a significant amount of energy before final failure is achieved. During this second, ductile failure stage partially polymerized poly(DCPD) fibrils that bridge the crack plane provide a means of load transfer between the two halves of the sample (Figure 1.3b).

In-situ samples were tested in a similar fashion to the self-activated samples, but no additional healing agent was manually applied in these cases. Rather, healing agent delivery is accomplished autonomically via fracture of microcapsules contained within the sample.

1.2 Results

a) Environmental Stability of WCl_6

Figure 1.4 contains the UV-vis spectra for the different WCl_6 forms investigated. The initial spectra for the as-received and recrystallized compound are consistent with published results (Thorn-Csányi & Timm 1985). After exposure to ambient air for 2 hours, about half of the as-received WCl_6 remains while the recrystallized WCl_6 has been completely converted to either $WOCl_4$ (as evidenced by the single peak at 355 nm reported by Thorn-

Csányi & Timm 1985) or other nonabsorbing or insoluble compounds. The spectra for the wax-protected WCl_6 is qualitatively different with a significant absorption band above 500 nm. Complexes of WCl_6 with phenols have been reported to have similar absorption spectra (Balcar *et al.* 1992), so this suggests that the tungsten in the wax-protected catalyst exists as a complex with the nonylphenol that is added. The as-received WCl_6 retained some presumably active $WOCl_4$ after 24 hours of exposure while the recrystallized and wax encapsulated forms retained no WCl_6 or $WOCl_4$.

b) Healing of the Self-Activated System

Self-activated tests were performed to demonstrate and refine the system. Specifically they were used to evaluate (i) the effect of WCl_6 delivery methods, (ii) the effect of a coupling agent on the virgin toughness, and (iii) the effect of the dispersion of the WCl_6 on the self-healing performance. Table 1.2 summarizes the results of these experiments.

Effect of WCl_6 Delivery Methods: Self-activated TDCB specimens with 4.4, 7 or 12 wt% of as-received or recrystallized WCl_6 were tested. The virgin and the initial portion of the healed load-displacement data for the 7 and 12 wt% samples were linear (Figures 1.3a and 1.3b) and therefore satisfied the requirements for the use of Eq. 1.2. To account for the large amount of energy consumed in the second stage of failure of these samples, we also calculated healing efficiencies using Eq. 1.3 for all sample types. The 4.4 wt% samples containing recrystallized WCl_6 and a coupling agent exhibited a non-linear healing response; therefore, Eq. 1.3 was used to quantify the healing efficiency. The polymerized healing agent was removed from the crack plane and analyzed by Fourier transform infrared spectroscopy (FTIR). By monitoring the spectra and observing the characteristic peak at 965 cm^{-1} corresponding to the *trans* double bond for both the polymerized healing agent and an authentic poly(*exo*-DCPD) control, it was confirmed that the achieved healing was a result of ROMP of *exo*-DCPD.

Self-activated TDCB samples containing 20 wt% of wax encapsulated WCl_6 (4.4 wt% overall catalyst loading) were also evaluated. A non-linear healing response (see Figure 1.3c) was obtained and the healing efficiency was evaluated using Eq. 1.3. The non-linearity upon healing in this case is likely due to either plasticization of the healed poly(DCPD) film by dissolved wax (Rule *et al.* 2007) or to incomplete polymerization as a result of the lower effective catalyst concentration as was exhibited in the 4.4 wt% recrystallized catalyst samples.

Effect of Coupling Agent: A decrease in the virgin fracture toughness was observed for both the as-received and recrystallized WCl_6 samples as shown in Table 1.2. In both cases, regardless of WCl_6 concentration, a large (ca. 50%) decrease in virgin fracture toughness occurs compared to neat resin. The size, shape, concentration and bonding of the particles to the matrix were all considered as possible causes for the decrease in toughness, but poor interfacial bonding between the WCl_6 and epoxy matrix was thought to be the prevailing effect. There is precedence in the literature for a decrease in fracture toughness of polymers due to poor adhesion of inclusions (Brown *et al.* 2004; Maiti & Sharma 1992; Wong & Truss 1994). Other factors such as particle shape, size, volume fraction, and distribution may also decrease toughness (Lange & Radford 1971; Quazi *et al.* 1999) and may account for the difference between the neat resin samples and the WCl_6 samples containing coupling agent.

To confirm that poor interfacial bonding between the WCl_6 and matrix was the dominant cause of decreased fracture toughness, a series of experiments were carried out with and without adhesion promoter. During manufacturing, 1 wt% of the silane coupling agent 3-glycidoxypropyltrimethoxysilane (Aldrich) was added to the epoxy resin prior to addition of the WCl_6 phase. A series of control samples with 1 wt% coupling agent, but no WCl_6 phase was also tested.

Control experiments confirmed that the addition of coupling agent has no effect on the fracture toughness of the neat epoxy. More importantly, the addition of the coupling agent increased the toughness of the as-received and recrystallized WCl_6 samples almost to levels consistent with the neat epoxy samples. Scanning electron images comparing the fracture surfaces of samples with and without coupling agent are shown in Figure 1.5. Debonding between the WCl_6 and matrix phase is clearly evident in the sample without coupling agent and it is dramatically suppressed when the coupling agent is added. A subset of the self-activated samples containing coupling agent was tested and a representative load vs. displacement response for these samples is shown in Figure 1.6. The healing for both types of WCl_6 delivery was unaffected by the addition of the coupling agent, as shown in Table 1.2.

Effect of Dispersion: The as-received form of the WCl_6 has a tendency to agglomerate into large particle clusters in the epoxy resin during processing and the lack of uniform dispersion leads to inconsistent healing. In order to obtain better dispersion, as-received WCl_6 was incorporated in the epoxy resin using a mechanical mixer stirring at 500 rpm prior to pouring into the molds.

SEM images of samples with and without mechanical mixing are compared in Figure 1.7. Image analysis was performed to ascertain the relative level of clustering of the WCl_6 particles. A method outlined by Schwarz and Exner (1983) to characterize the clustering of points was implemented. The distance from the centroid of each cluster to its nearest neighbor was calculated. The mean and variance of the distribution of distances was calculated for samples with and without mechanical mixing as well as a random distribution from a Poisson point process with the same number of particles and image size as each image. The parameters Q and R were calculated as

$$Q = \frac{\bar{r}_{image}}{\bar{r}_{random}} \tag{1.4}$$

and

$$R = \frac{\sigma^2_{image}}{\sigma^2_{random}} \tag{1.5}$$

where $\bar{r}_{image}$ and $\bar{r}_{random}$ are the mean distances to nearest neighbors for the image of interest and the random distribution, respectively, and the σ^2_{image} and σ^2_{random} are the variances of the distribution of distances to nearest neighbors of the image of interest and the random distribution.

Deviation of Q or R from unity indicates some degree of clustering and was used to characterize the relative clustering between the two mixing conditions. Table 1.3 summarizes the results from this analysis. The Q and R values for the mechanically mixed sample both deviated from unity by less than 7%. When no mechanical mixing was used image analysis yields Q=0.85 and R=1.74 indicative of significant clustering of catalyst particles. Interestingly, the healing efficiency of the well dispersed WCl_6 samples dropped from 107% to 20% and the healing response was non-linear, as shown in Figure 1.8.

c) Self-healing of the In-Situ Microencapsulated System

In-situ healing experiments were performed with 12 wt% recrystallized WCl_6 and 15 wt% microcapsules that contained a healing solution of *exo*-DCPD, nonylphenol, and phenylacetylene at the same concentrations as the self-activated healing solution. The healed samples exhibited a non-linear fracture response, as shown in Figure 1.9a, indicating incomplete polymerization of the poly(DCPD) film. Figure 1.9b shows a representative SEM image of the fracture surface after healing of an *in-situ* sample. Broken microcapsules and poly(*exo*-DCPD) film are present on the fracture surface indicating that mechanical triggering of the monomer release occurred. Healing efficiency calculated using Eq. 1.3 is 20%.

1.3 Discussion

Self-activated TDCB experiments clearly demonstrate the effectiveness of WCl_6 as a catalyst precursor for self-healing epoxy. Of the delivery methods examined, the as-received morphology retains the greatest activity upon exposure to laboratory air. The surface area to volume ratio of the particles may play an important role in the environmental stability of the particles. Table 1.1 shows the surface area to volume ratio for each of the three WCl_6 forms. The as-received and recrystallized forms have similar surface areas per unit volume indicating that the difference in stability is not directly attributed to the surface area, but may be dictated by the smallest critical dimension. As the outer surface oxidizes, more of the WCl_6 remains active in the as-received particles with a larger critical dimension (27.8 μm) in comparison to the recrystallized particles with the smaller critical dimension (11.8 μm). Wax-protection of the WCl_6 phase achieved mixed results – healing was obtained for effective WCl_6 concentrations that were lower than could be obtained by other delivery methods (4.4 wt%), but no healing activity could be detected after 24 h exposure to laboratory air.

Inherently coupled to the deactivation problem, dispersion of the WCl_6 phase within the epoxy matrix plays an important role in the efficiency of healing. Healing activity is preserved via particle clustering – presumably by sealing interior particles from exposure to the surrounding polymer matrix. When these clusters are broken up and dispersed through strong mechanical mixing, the healing efficiency dramatically decreased. Embedding the WCl_6 phase in wax leads to better dispersion while maintaining reasonable healing efficiency.

For the as-received and recrystallized delivery methods, more than 7 wt% WCl_6 loading was necessary to achieve complete healing. Some portion of the WCl_6 was deactivated during specimen manufacturing and curing. Hence, better protection schemes will enable lower tungsten loadings in the future. Even with the technical challenges identified, *in-situ* healing was demonstrated (ca. 20%) using 12 wt% as-received WCl_6 and 15 wt% microcapsules containing *exo*-DCPD healing agent. More effective protection schemes for WCl_6 and other co-activators mixed with the healing agent are being examined for further enhancement of this self-healing system.

1.4 Conclusions

A cost-effective way to achieve self-healing was achieved using WCl_6 with a co-activator (phenylacetylene) that initiates ROMP of *exo*-DCPD. The environmental stability of three WCl_6 delivery methods was investigated by UV-vis spectrophotometry and the as-received form shows the greatest stability after 24 h exposure to laboratory air. Self-activated healing of TDCB fracture specimens showed nearly complete recovery for 12 wt% catalyst loading for both as-received and recrystallized WCl_6, but strong mechanical mixing to promote dispersion of the catalyst reduced healing efficiency dramatically. The virgin

fracture toughness of epoxy was reduced by approximately 48% upon addition of WCl_6 particles and this reduction was attributed to poor interfacial bonding. Incorporating a silane coupling agent into the matrix resin increased the virgin fracture toughness to about 75 % of the neat resin toughness. Preliminary *in-situ* healing experiments using 12 wt% as-received WCl_6 and 15 wt% 188 μm microcapsules containing *exo*-DCPD healing agent, 0.5 wt% phenylacetylene and 1.0 wt% nonylphenol yielded ca. 20% healing efficiency. Further research is required to optimize the healing efficiency by more effective WCl_6 protection schemes, more efficient co-activators, and enhanced processing methods to achieve uniform WCl_6 dispersion.

1.5 References

Balcar, H., Dosedlová, A. & Petrusová, L. 1992 Ring-opening metathesis polymerization of dicyclopentadiene by unicomponent catalysts derived from WCl_6. *Journal of Molecular Catalysis* **77**, 289-295. (DOI 10.1016/0304-5102(92)80208-X)

Breslow, D. S. 1990 How we made neat stuff. *Chemtech*, **20**, 540-544.

Brown, E.N., Kessler, M.R., Sottos, N. R. & White, S. R. 2003 In situ poly(urea-formaldehyde) microencapsulation of dicyclopentadiene. *Journal of Microencapsulation* **20**, 719-730. (DOI 10.1080/0265204031000154160)

Brown, E.N., Sottos, N.R., & White, S.R. 2002 Fracture testing of a self-healing polymer composite. *Experimental Mechanics* **42**, 372-379. (DOI 10.1177/001448502321548193)

Brown, E.N., White, S.R., & Sottos, N.R. 2004 Microcapsule induced toughening in a self-healing polymer composite. *Journal of Materials Science* **35**, 1703-1710. (DOI 10.1023/B:JMSC.0000016173.73733.dc)

Chen, X., Dam, M.A., Ono, K., Mal, A., Shen, H., Nutt, S.R., Sheran, K., & Wudl, F. 2002 A thermally re-mendable cross-linked polymeric material. *Science* **295**, 1698-1702. (DOI 10.1126/science.1065879)

Cho, S.H., Andersson, M.H., White, S.R., Sottos, N.R., & Braun, P.V. 2006 Polydimethylsiloxane-based self-healing materials. *Advanced Materials* **18**, 997-1000. (DOI 10.1002/adma.200501814)

Fratzl, P. 2007 Biomimetic materials research: what can we really learn from nature's structural materials? *Journal of the Royal Society Interface* Published Online. (DOI 10.1098/rsif.2007.0218)

Katz, T. J. & Han, C. C. 1982 Induction of olefin metathesis by phenylacetylene plus tungsten hexachloride. *Organometallics* **1**, 1093-1096. (DOI 10.1021/om00068a019)

Ketelaar, J. A. A. & van Oosterhout, G. W. 1943 Die krystallstruktur des wolframhexachlorids. *Recueil des Travaux Chimiques des Pays-Bas et de la Belgique* **62**, 197-200.

Lange, F.F. & Radford, K.C. 1971 Fracture energy of an epoxy composite system. *Journal of Materials Science* **6**, 1197-1203. (DOI 10.1007/BF00550203)

Maiti, S.N. & Sharma, K.K. 1992 Studies on polypropylene composites filled with talc particles. I. Mechanical properties. *Journal of Materials Science* **27**, 4605-4613. (DOI 10.1007/BF01165994)

Mauldin, T.C., Rule, J.D., Sottos, N.R., White, S.R., & Moore, J.S. 2007 Self-healing kinetics and the stereoisomers of dicyclopentadiene. *Journal of the Royal Society Interface* **4**, 389-393. (DOI 10.1098/rsif.2006.0200)

Nelson, G.L. & Kuo, C.L. 1975 An improved procedure for the preparation of *exo*-dicyclopentadiene. *Synthesis* **105**, 105-106. (DOI 10.1055/s-1975-23674)

Pang, J. W. C. & Bond, I. P. 2005 A hollow fibre reinforced polymer composite encompassing self-healing and enhanced damage visibility. *Composites Science and Technology* **65**, 1791-1799. (DOI 10.1016/j.compscitech.2005.03.008)

Quazi, R.T., Bhattacharya, S.N. & Kosior, E. 1999 Effect of dispersed paint particles on the mechanical properties of rubber toughened polypropylene composites. *Journal of Materials Science* **34**, 607-614. (DOI 10.1023/A:1004515300637)

Rule, J. D. 2005 Polymer Chemistry for Improved Self-Healing Composite Materials. PhD Thesis, University of Illinois at Urbana-Champaign, Urbana, IL.

Rule, J. D., Brown, E. N., Sottos, N. R., White, S. R. & Moore, J. S. 2005 Wax-protected catalyst microspheres for efficient self-healing materials. *Advanced Materials* **17**, 205-208. (DOI 10.1002/adma.200400607)

Rule, J.D., Sottos, N.R., & White, S.R. 2007 Effect of Microcapsule Size on the Performance of Self-Healing Materials. *Polymer*. Article in Press. (DOI:10.1016/j.polymer.2007.04.008)

Schwarz, H. & Exner, H.E. 1983 The characterization of the arrangement of feature centroids in planes and volumes. *Journal of Microscopy* **129**, 155-169.

Shriver, D.F. & Drezdzon, M.A. 1986 *The Manipulation of Air-Sensitive Compounds, 2nd Edition,* New York, Wiley-Interscience.

Sottos, N.R., White, S.R. & Bond, I.P. 2007 Self-healing polymers and composites, Papers of a themed supplement, **4**, 347-411.

Thorn-Csányi, E. & Timm, H. 1985 Kinetic studies of the system tungsten hexachloride/tetramethyltin (diethyl ether)/C_5-olefins; determination of the initial reaction steps. *Journal of Molecular Catalysis* **28**, 37-48. (DOI 10.1016/0304-5102(85)87016-4)

Toohey, K., Lewis, J.A., Moore, J.S., White, S.R. & Sottos, N.R. 2007 Self-healing materials with microvascular networks. *Nature Materials*. Accepted for publication.

White, S. R., Sottos, N. R., Geubelle, P. H., Moore, J. S., Kessler, M. R., Sriram, S. R., Brown, E. N., & Viswanathan, S. 2001 Autonomic healing of polymer composites. *Nature* **409**, 794-797. (DOI 10.1038/35057232)

Wong, K. W.Y. & Truss, R.W. 1994 Effect of flyash content and coupling agent on the mechanical properties of flyash-filled polypropylene. *Composites Science and Technology* **52**, 361-368. (DOI 10.1016/0266-3538(94)90170-8)

Table 1.1 Size distributions for WCl_6 delivery methods.

WCl_6 Delivery Method	Mean Size (μm)	Standard Deviation (μm)	Area/Volume (μm^{-1})
As-Received	27.8	7.9	0.21
Recrystallized	61.8 (planar) 11.8 (thickness)	43.6 7.0	0.22
Wax Protected	103.2	56.5	0.06

Table 2. Summary of healing efficiencies for the three WCl_6 delivery methods and the effect of coupling agent on fracture toughness.

Sample Type	No. of Samples	WCl_6 Loading (wt%)	Coupling Agent (wt%)	K_{Ic}^{virgin} (MPa·m$^{1/2}$)	K_{Ic}^{healed} (MPa·m$^{1/2}$)	η (%)	η' (%)
Neat Resin	8	0	0	0.84 ± 0.06	-	-	-
Neat Resin	8	0	1	0.85 ± 0.08	-	-	-
As-Received	5	7	0	0.44 ± 0.11	0.20 ± 0.09	46	187
As-Received	6	12	0	0.44 ± 0.03	0.47 ± 0.07	107	263
As-Received	4	12	1	0.67 ± 0.14	0.52 ± 0.14	78	247
Recrystallized	7	4.4	1	0.55 ± 0.10	NL**	-	11
Recrystallized	4	7	0	0.37 ± 0.04	0.17 ± 0.04	46	160
Recrystalllized	7	12	0	0.41 ± 0.06	0.37 ± 0.12	90	231
Recrystallized	5	12	1	0.66 ± 0.09	0.44 ± 0.09	67	204
Wax Protected*	4	4.4	0	0.60 ± 0.05	NL**	-	49
*In-situ***	3	12	0	0.85 ± 0.06	NL**	-	20

* 20 wt% wax beads in epoxy resin with 22 wt% WCl_6 concentration in wax
** NL = Non-linear healing response
*** 15 wt% microcapsules of *exo*-DCPD/phenylacetylene/nonylphenol

Table 3. Summary of cluster parameters of samples with and without mechanical mixing.

Sample Type	$\bar{r}$ (μm)	σ^2 (μm^2)	Q	R
Random Distribution*	149.4	6,100.8	1.00	1.00
With Mechanical Mixing	142.3	5,659.5	0.95	0.93
Random Distribution**	147.6	5,954.0	1.00	1.00
Without Mechanical Mixing	126.1	10,387.2	0.85	1.74

* based on image from Figure 1.7a
** based on image from Figure 1.7b

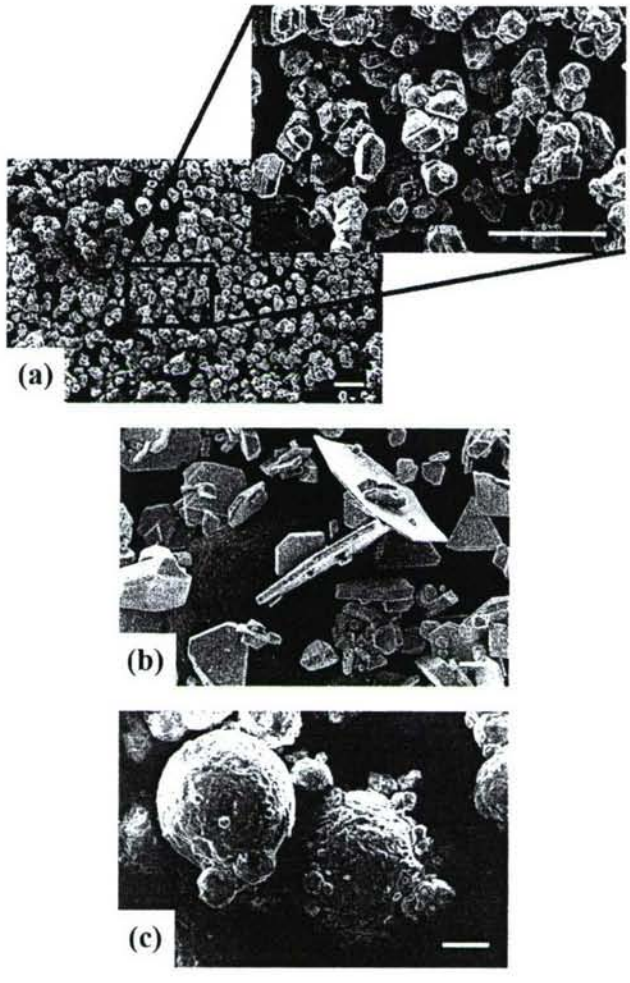

Figure 1.1 Scanning electron microscope (SEM) images of WCl_6. a. as-received, b. recrystallized and c. wax protected. [scale bars = 100 μm]

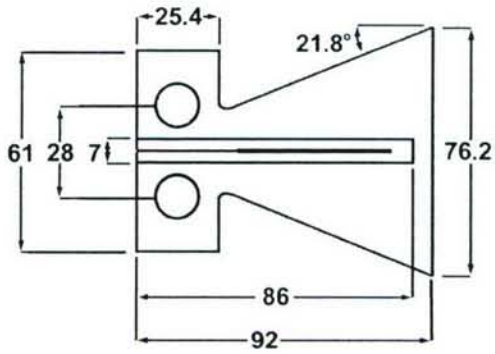

Figure 1.2. Localized TDCB specimen geometry (all dimensions in mm) (Rule *et al.* 2007).

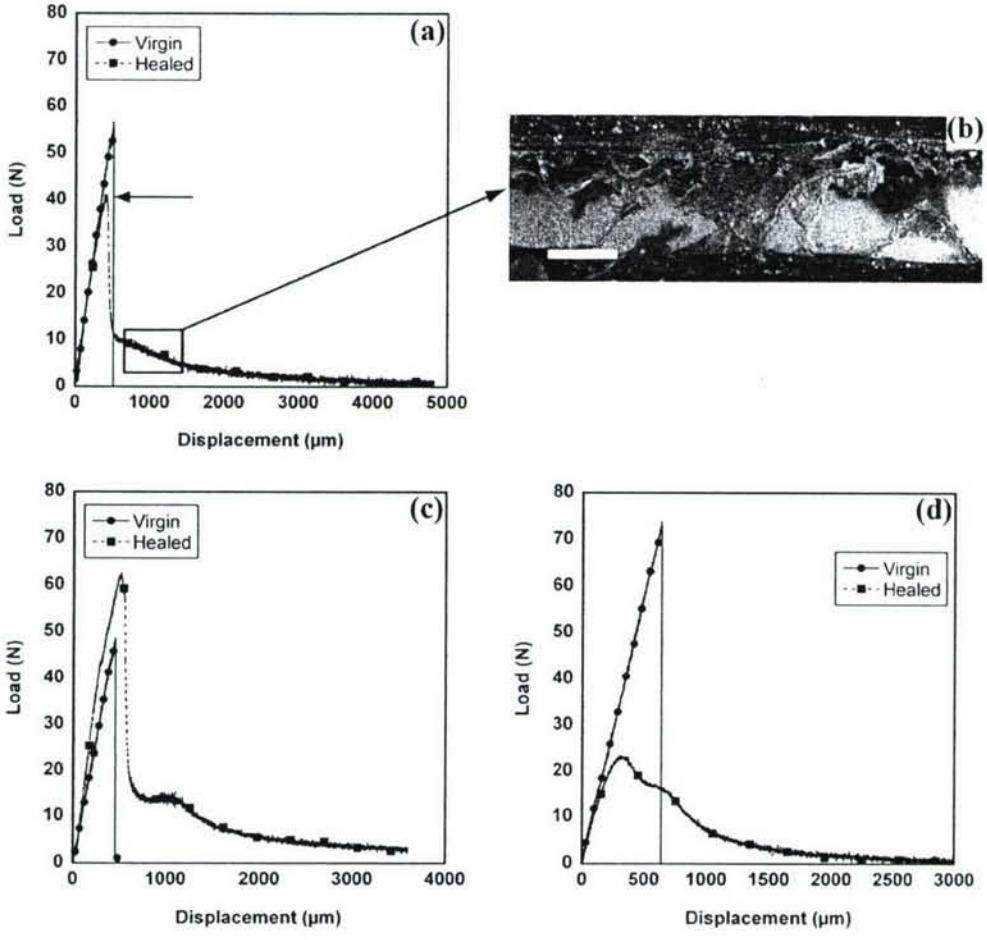

Figure 1.3. Mechanical assessment of self-activated specimens. a. Representative load vs. displacement data for recrystallized specimens (arrow indicates the peak of the healed response). b. Image of poly(DCPD) fibrils spanning the fracture plane (scale bar = 1 mm) c. Representative load vs. displacement data for as-received specimens. d. Representative load vs. displacement data for wax protected samples.

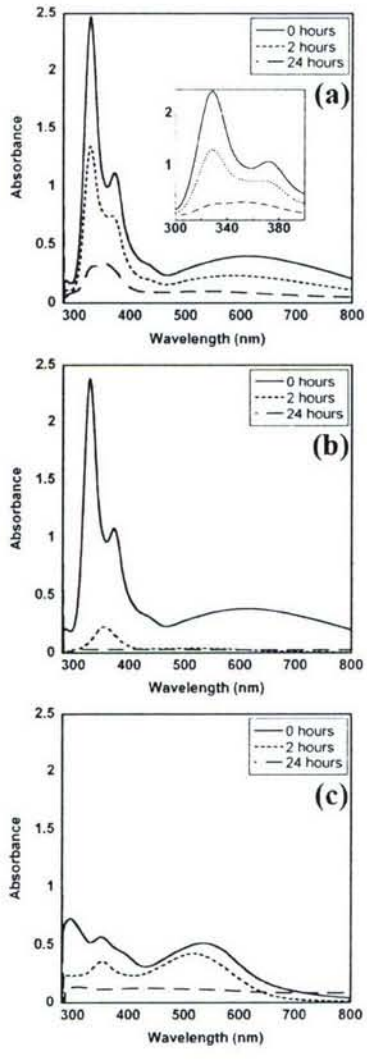

Figure 1.4. UV-vis spectra results for a. as-received with inset of spectra from 300-400 nm, b. recrystallized, and c. wax protected WCl_6 upon exposure to air at 22 °C and 30 % relative humidity for 0, 2, and 24 hours. The characteristic peaks for WCl_6 are located at 328 and 372 nm, and for $WOCl_4$ at 355 nm (Thorn-Csányi & Timm 1985).

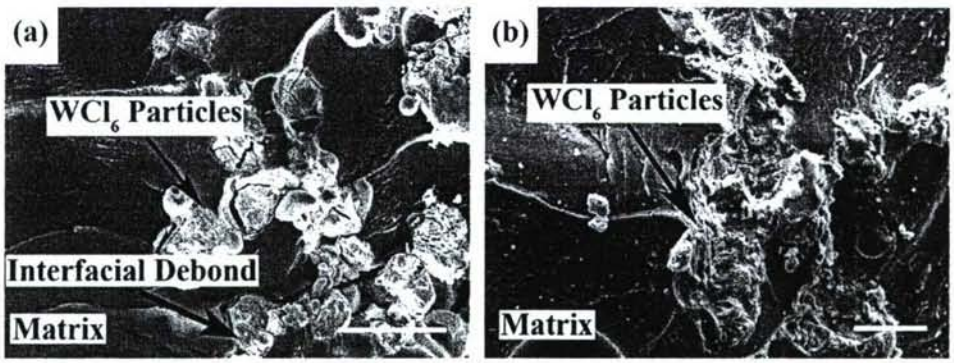

Figure 1.5. SEM images of epoxy fracture surfaces for samples containing as-received WCl_6 (12 wt%). a. Significant interfacial debonding is revealed when no coupling agent is used. b. The addition of 1 wt% silane coupling agent (3-glycidoxypropyltrimethoxysilane) dramatically reduces the amount of interfacial debonding. [scale bars = 50 μm]

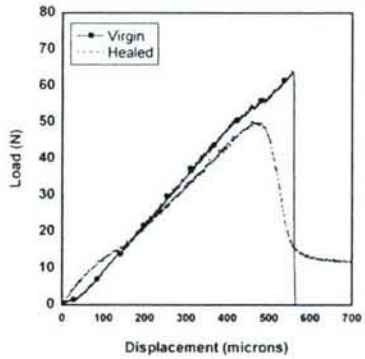

Figure 1.6. Self-activated mechanical response of a sample containing 12 wt% recrystallized WCl_6 with 1 wt% coupling agent in the matrix.

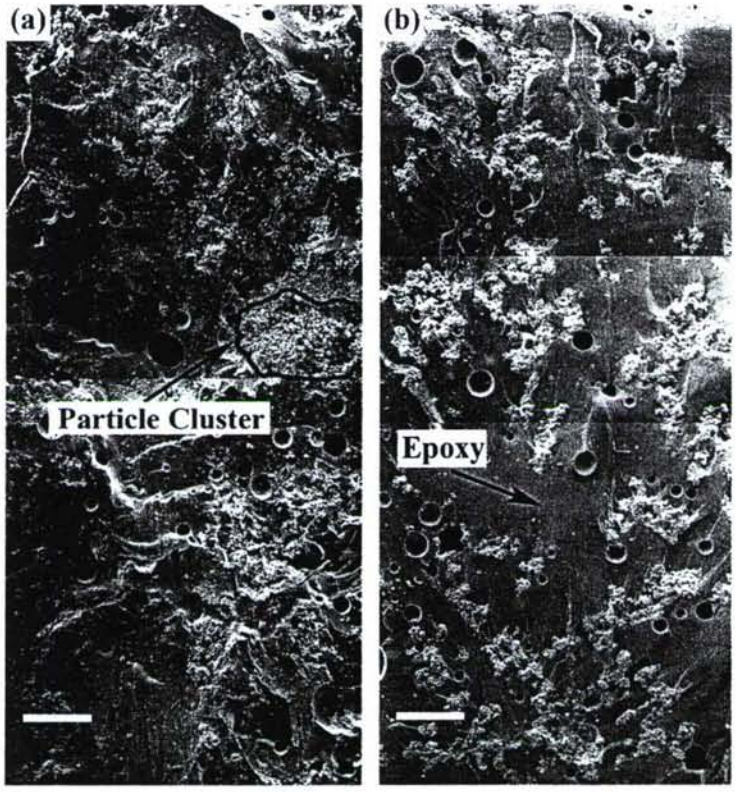

Figure 1.7. SEM images of epoxy fracture surfaces for samples containing as-received WCl_6 (12 wt%). a. Significant clustering of tungsten particles in the absence of mechanical mixing. b. Particle dispersion achieved by mechanical mixing at 500 RPM. [scale bars = 500 μm]

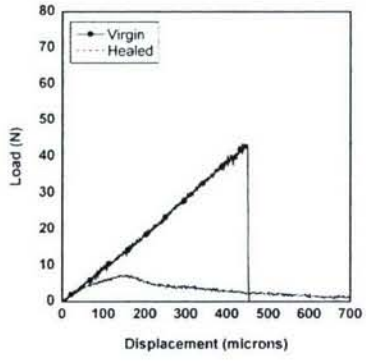

Figure 1.8. Self-activated mechanical response of a sample containing 12 wt% as-received WCl_6 dispersed with mechanical mixing at 500 RPM.

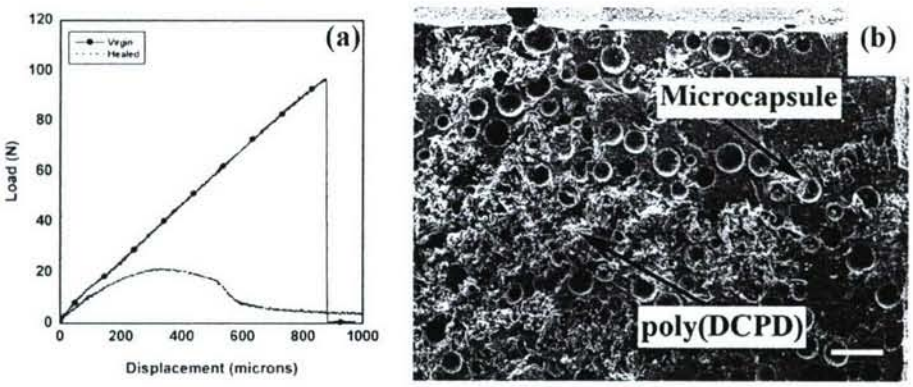

Figure 1.9. a. *In-situ* mechanical response of a sample containing 12 wt% recrystallized WCl_6 and 15 wt% 188 $\pm$ 31 μm capsules and b. SEM image of the fracture surface of an *in-situ* sample after healing and refracture. [scale bar = 500 μm]

2. Benzocyclobutene-based Mechanochemical Triggers

2.1 General Chemistry of Benzocyclobutenes

The use of benzocyclobutenes in both small molecule and polymer synthesis has been recently reviewed (Segure and Martin, 1999). Benzocyclobutenes undergo reversible ring opening of the four-membered ring to yield extremely reactive *ortho*-quinodimethane (*o*QDM) intermediates, which readily undergo Diels-Alder cycloadditions with dienophiles. Ring opening occurs predominately by a conrotatory pathway (Huisgen and Seidl, 1964), consistent with the predictions of the Woodward-Hoffman rules. Sakai has estimated that there is a 7-8 kcal/mol preference for conrotatory ring opening over disrotatory ring opening using calculations at the CASSCF level (Sakai, 2000). Roth has suggested that disrotatory ring opening occurs through a diradical intermediate (Roth *et al.*, 1996). To support this, he estimated that the enthalpy of the transition state (TS) for the forbidden, concerted disrotatory ring opening and the energy for geometric isomerization of the methylene carbons through a biradical intermediate were nearly the same. In other words, radical cleavage of the four-membered ring yields a stabilized diradical intermediate, which then relaxes to an *o*QDM intermediate. This process results in a formal disrotatory ring opening.

It is well documented that benzocyclobutenes prefer conrotatory ring opening; however it has been found that, quite often substituents on the four-membered ring strongly prefer to rotate either "inward" or "outward" to accomplish ring opening. This effect has been called "torquoselectivity" by Houk (Kirmse *et al.*, 1984; Rondan and Houk, 1985). He and others have found a strong preference for electron donating substituents to rotate outwards and for electron withdrawing substituents to rotate inwards in both cyclobutenes (Kirmse *et al.*, 1984; Rondan and Houk, 1985; Spellmeyer and Houk, 1988) and benzocyclobutenes (Jefford et al., 1992; Mariet et al., 2004). It is proposed that this is due to the favorable interaction of a donor group with the empty LUMO of the transition state for ring opening upon outward rotation, thereby stabilizing the transition state and assisting in bond breaking. However, upon rotation of a donor group inwards, there is an unfavorable interaction with the filled HOMO of the transition state, thereby destabilizing the transition state for ring opening. Thus, there is a significantly lower energy of activation for the outward rotation of an electron donating group. The opposite effect is found for an electron withdrawing group; inward rotation is stabilized by the interaction of the empty orbital on the acceptor substituent with the filled HOMO of the transition state, and therefore the energy of activation for inward rotation is lowered. The overall preference for outward or inward rotation can be quite powerful; Houk has calculated that there is a 14 kcal/mol preference for outward rotation of methoxy-substituted cyclobutenes (Kirmse *et al.*, 1984).

After ring opening, the *o*QDM intermediate typically cannot be isolated and quickly reacts through a number of pathways. In the absence of a dienophile trap, the *o*QDM intermediate will dimerize through a formal [4+4] pathway to yield dibenzocyclooctadienes, or through a formal [4+2] pathway to a spiro dimer (Errede, 1961). However, in the presence of an activated dienophile, cycloaddition occurs significantly faster than dimerization (Segure and Martin, 1999).

2.2 Benzocyclobutenes as Mechanochemical Triggers

We propose that benzocyclobutenes are well-suited as mechanochemical triggers. Mechanical tension across the 1-2 carbon-carbon bond in the four-membered ring could promote ring opening of the benzocyclobutene, which yields an *o*QDM intermediate after rearrangement (Figure 2.1). This intermediate could then react with pendant dienophiles in the polymer backbone to create new carbon-carbon bonds in the local region of stress

without first breaking the polymer backbone. Furthermore, the thermal energies of activation for electrocyclic ring opening of benzocyclobutenes are in the range of 25-45 kcal/mol (Jefford *et al.* , 1992), well below the energy needed for carbon-carbon bond homolysis. The following sections summarize the computational studies, synthesis, and reactivity of benzocyclobutene-based mechanochemical triggers.

2.3 Computational Studies on Trigger Design

a. Effect of Stress on Benzocyclobutenes

In order for stress to reduce the barrier to the reactive *o*QDM intermediate, it needs to distort the trigger so that the new conformation is nearer to the transition state of the thermal ring opening reaction. The stress-induced deformations are conveniently studied and optimized computationally using the COGEF technique (Beyer, 2000). A profile of change in ground state energy (ΔE_{GS}) vs molecular elongation was used to investigate the consequences of applied stress on the conformations and energies of benzocyclobutene triggers (Figure 2.2). To produce these curves, the distance *d* between the methyl carbons of *trans* or *cis* 1,2-diethylbenzocyclobutene was fixed and all other atoms were allowed to fully relax. After relaxation, the energy was calculated at the B3LYP/6-31G* level.[1,2] Distance *d* was systematically increased and the energy at each interval was calculated. In these profiles, stress-induced reactions appear as drops in energy with a corresponding change in geometry to a structure consistent with a *o*QDM. The difference in the thermal activation energy and the amount of work needed to bring about reaction can also be compared by calculating the energy of the thermal transition state (E_{TS}) and the ground state, then calculating the energy of activation using Eq. 2.1:

$$E_A = E_{TS} - E_{GS} . \qquad (2.1)$$

The comparison between the thermal E_A for electrocyclic ring opening and the amount of work needed to induce ring opening provides some indication about the extent of congruency between the thermal and mechanochemical pathways. It is assumed that the amount of work done on the molecule by stress is equal to the ground state energy increase.

These studies revealed that the *trans* and *cis* isomers respond quite differently to applied stress. Ring opening in the *trans* isomer is efficiently activated by tensile stress as indicated by a drop in energy after 13% elongation, and a corresponding new geometry that is consistent with the expected *o*QDM. Comparison of the thermal E_A and the amount of work necessary to induce ring opening suggests that the thermal and mechanical reaction pathways are highly congruent (E_A is 43 kcal/mol in the thermal reaction versus 45 kcal/mol of work in the stress reaction, relative to the undistorted ground state).

In contrast, the electrocyclic ring opening of the *cis* isomer is predicted to be retarded by applied stress. The profile of relative energy versus percent elongation indicate that a rearrangement occurs after 94 kcal/mol of work is done on the molecule by stress, while only 47 kcal/mol of thermal energy is needed to open the ring. Furthermore, the reaction requires twice as much distortion as the *trans* isomer, occurring after 26% backbone elongation. These results indicate that the thermal and mechanical pathways in the *cis* isomer are not congruent.

---

[1] Calculations were completed using Spartan 04, Wavefunction, Inc.

[2] It is realized that DFT often fails for the calculations of some reaction barriers, particularly so when bonds are significantly distorted. However, we were more interested in the effect of stress on the deformations of benzocyclobutenes, and not the reaction energies.

The reactivity difference between the *cis* and *trans* isomers has been attributed to effective torque (Figure 2.3). In *trans*-benzocyclobutene, the applied stress vector induces a conrotatory motion of the substituents. This motion is congruent with the intended thermal reaction and facilitates the thermally allowed conrotatory ring opening. However, in the *cis* isomer, stress induces a disrotatory motion. This opposes the thermally allowed conrotatory electrocyclic ring opening. Because the thermal and mechanical processes are in opposition, both E_{GS} and E_{TS} increase until some other reaction pathway becomes competitive. In this case, the competing thermal reaction is proposed to be a radical fragmentation of the benzocyclobutene ring, which then can relax to the same E,E-*o*QDM intermediate from the thermal conrotatory rearrangement of the *trans* isomer to result in a formal disrotatory ring opening of the *cis* isomer. The overall prediction of the computational study is that elongational stress will promote the conversion of both isomers to the same E,E-*o*QDM intermediate, but with different reaction energies.

There is an interesting consequence of induced torque in the presence of a stress field. It is well known that disrotatory ring opening is a thermally disallowed process for benzocyclobutenes under thermal conditions, and therefore is a higher energy process relative to the allowed conrotatory process. Since tensile stress applied to the *cis* isomer induces a disrotatory motion, we were intrigued by the possibility that stress could promote a formal disrotatory process in preference to a formal conrotatory process in a *cis* benzocyclobutene.

b) Effect of Substituents on Electrocyclic Ring Opening

Electrocyclic ring opening of benzocyclobutenes is known to be accelerated by electron donating groups and inhibited by electron withdrawing groups relative to the parent unsubstituted benzocyclobutene (Jefford *et al.*, 1992). Therefore, it was hypothesized that the energy of activation could be controlled with proper choice of substituents. It is desirable for mechanochemical triggers to have thermal energy of activations in the range of 25-35 kcal/mol. To assist in choosing the correct substituent, the effect of substitution on E_A was examined computationally.

In order to study the substituent effect properly, a reliable computational technique needed to be developed. We decided to start with calculations at the DFT B3LYP/6-31G* level because they were previously shown to be successful in the study of enediynes. To test this model's ability to reproduce E_A for electrocyclic ring opening, the effect of substituents for ring opening of cyclobutenes was examined. Three examples of disubstituted cyclobutenes were modeled which had empirically-determined E_A values (Table 2.1) (Kirmase et al., 1984). The E_A for each of the structures was calculated at the DFT B3LYP/6-31G* level by calculating E_{GS} and E_{TS} for each species. The E_A was then calculated using Eq. 2.1.

The values for E_A obtained computationally were similar to experimental values. The standard deviation of the error between the calculated and experimentally reported values was 5%, and the maximum was 11%. This demonstrates that the DFT B3LYP/6-31G* model chosen is reliable for calculating the energies for electrocyclic ring opening.

With a sufficient computational technique in hand, the effect of several substituents on the E_A of *trans*-1,2-disubstituted benzocyclobutenes was calculated (Table 2.2). Of the three substituents that provided activation energies within the target range, the diester substituted benzocyclobutene was chosen as an ideal first target because it was anticipated that the symmetry in this molecule would make its preparation easier. Thus, as initial targets, benzocyclobutene linkers **1** and **2** were chosen.

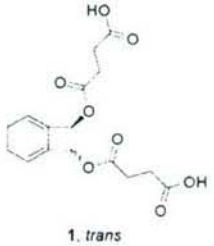

1. *trans*
2. *cis*

2.4 Preparation of Substrates

a. Preparation of Benzocyclobutene Linkers

trans-Benzocyclobutene linker **1** was prepared starting from benzocyclobutene-1,2-dione **3** (South and Lesbeskind, 1982), which was reduced (Allen *et al.*, 2000) to yield a mixture of the *trans*:*cis* diols in a 4:3 ratio (Scheme 2.1). These were separated by column chromatography at 4 °C in a cold room. The unstable *trans* diol, which polymerizes at room temperature (Nozaki *et al.*, 1964), was then immediately trapped with acid **4** (Pouzair et al., 1984) under carbodiimide coupling conditions at 0 °C to yield benzocyclobutene **5**. Deprotection of ester **5** with TBAF then yielded *trans* linker **1**. The amount of *cis*-benzocyclobutene impurity was estimated to be < 5% by ^{1}H NMR integration. Unlike the diol, ester **1** is thermally stable for extended time at room temperature.

Scheme 2.1. Preparation of *trans*-benzocyclobutene linker **1**.

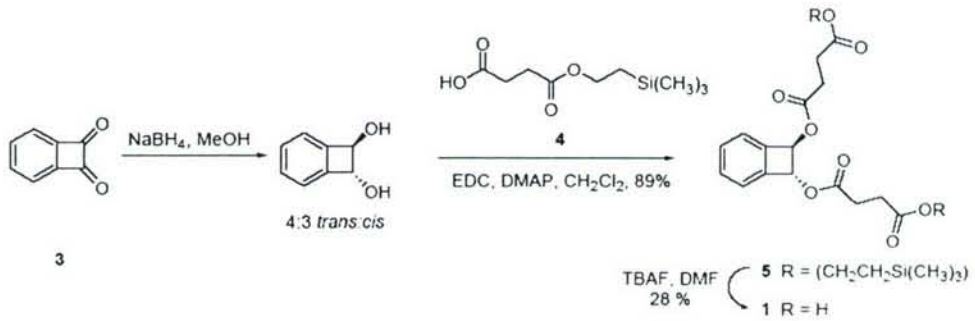

Preparation of the *cis*-benzocyclobutene linker began with *cis*-benzocyclobutene-1,2-diol (Nozaki *et al.*, 1964) (Scheme 2.2). The *cis* diol is much more stable than the *trans* isomer and this was esterified with acid **4** under carbodiimide coupling conditions at room temperature. Cleavage of the protecting group with TBAF yielded diacid linker **2** in 86% yield. The *cis* configuration of the substituents around the 4-membered ring was verified by single crystal x-ray analysis (Figure 5.4).

Scheme 2.2. Preparation of *cis*-benzocyclobutene linker **2**.

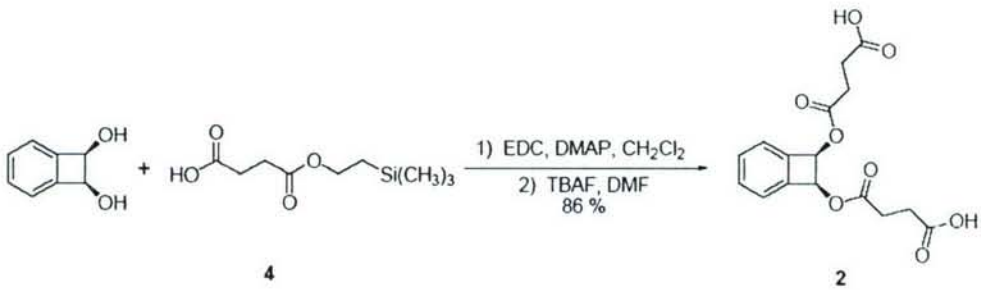

b. Preparation of Benzocyclobutene-Containing LFPs

When preparing LFPs with mechanochemical triggers, it is desirable to position the trigger near the center of the polymer chain, where solvodynamic forces are expected to be the greatest. Therefore, LFPs were prepared with low polydispersity α-methoxy-ω-amino poly(ethylene glycol) (mPEG) by coupling the chains to the acid residues on the linker

(Berkowski *et al.*, 2005). This yielded polymers **6** and **7**, which contained the *trans*-benzocyclobutene linker and the *cis*-benzocyclobutene linker, respectively, each with MW of 4, 10, 20, 40 and 60 kDa.

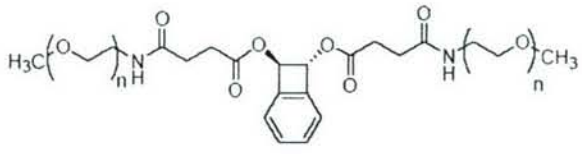

6

MW = 4, 10, 20, 40, 60 kDa

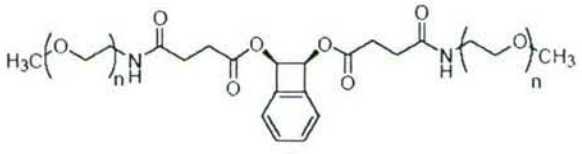

7

MW = 4, 10, 20, 40, 60 kDa

2.5 Demonstration of Mechanochemical Activation

a. Reactivity of 40 kDa Benzocyclobutene LFPs Under Ultrasound

Using conventional analytical techniques, it is difficult to observe one unique unit within a 40 kDa polymer. Therefore, N-(1-pyrene)-maleimide **8** (Reddy *et al.*, 1998) was chosen as a dienophile trap; the pyrene label allows the reaction to be monitored by GPC equipped with a UV detector. Since each polymer chain contains only a single mechanically sensitive unit, only a single pyrene label should be incorporated into each chain by cycloaddition of the trap to the *o*QDM generated after ring opening.

Since it has been previously demonstrated that ultrasound can be used to activate mechanically-sensitive LFPs in solution (Berkowski *et al.*, 2005), this technique was chosen to study the benzocyclobutene-containing LFPs. Therefore, a solution of 40 kDa LFP **6** or **7** in acetonitrile was sonicated in the presence of a 500-fold excess of trap **8**. External ice bath cooling maintained a temperature below 10 °C. After 45 min of pulsed ultrasound, the solvent was removed and the polymer was isolated by preparatory scale GPC. After isolation of the polymer, a GPC trace was obtained by monitoring the UV absorbance at 345 nm, a wavelength where the starting polymer has no absorbance but the pyrene-label strongly absorbs. The RI signal was also monitored and used as an internal standard. It was found that, after 45 min of sonication, the UV signal corresponding to unbroken 40 kDa chains significantly increased relative to the RI signal in both polymers **6** and **7** (Figure 2.5, a and b). This result suggested that pyrene label was incorporated into both LFPs, a surprising result given the predictions from calculations.

Several control experiments suggest that the increased response was due to the proposed stress-induced ring opening reaction followed by cycloaddition to trap **8**. First, no increase in UV absorbance was found when ultrasound was omitted, indicating that ultrasound is necessary for the observed response of LFPs **6** and **7** (Figure 2.6). Second, PEG polymer of MW 43 kDa, which contained no linker, was subjected to the same conditions as above. It was found that the UV absorbance was significantly less than that in the benzocyclobutene LFPs (Figure 2.5, c). This result suggests that incorporation of the labeled trap into polymers **6** and **7** is dependent on the presence of the benzocyclobutene linker.

b. Effect of Chain Length on Rate of Reaction

Demonstration of chain-length dependence on the rate of reaction supports a mechanochemical process. In particular, longer chains experience larger solvodynamic shear and therefore larger tensile force. If the force reduces a kinetic barrier to ring opening, larger force should correlate to a faster rate of reaction. A reaction promoted by thermal fluctuations or mass transfer effects is not expected to have this MW dependence. LFP **6** and **7** with MW of 4, 10, 20, and 60 kDa were sonicated in the presence of trap **8** as described above. The UV/RI signal ratios of unbroken chains were monitored by GPC and plotted vs MW (for GPC traces, see experimental section). It was found that for both LFPs **6** and **7**, the UV/RI signal ratio increased linearly with increasing MW (Figure 2.7). Surprisingly, *cis* LFP **6** was found to react faster than *trans* LFP **7** for all MW studied. The increasing response with increasing MW indicates that the reaction is a mechanochemical process and not thermal activation by ultrasound. As a control, a MW profile of PEG with MW 5, 10, 20, 26, and 60 kDa was also examined. In this case, the UV/RI ratio of the unbroken chains[3] is independent of MW. As a second control, a 1:1 mol ratio mixture of LFP **7** and 43 kDa PEG was sonicated. The characteristic increase in the UV signal found in 40 kDa LFPs was not observed (Figure 2.8). This result suggests that the linker must be imbedded within a polymer above the critical MW to observe reactivity; mixing alone is not enough.

Scheme 2.3. Preparation of ^{13}C-labeled maleimide **9**.

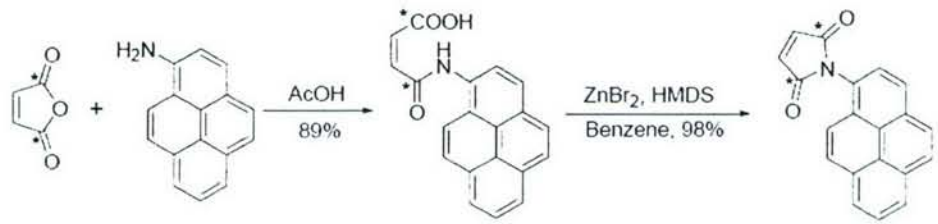

9

c. ^{13}C Labeling Studies

In order to further demonstrate that a stress-induced ring opening followed by cycloaddition occurs in LFPs **6** and **7**, and to investigate the stereochemical consequences of stress-activation, pyrene-labeled maleimide trap **8** was resynthesized to enrich the carbonyl carbons with ^{13}C isotope, yielding ^{13}C labeled trap **9** (Scheme 2.3). 40 kDa polymers **6** and **7** were subjected to ultrasound in the presence of maleimide trap **9**. After 45 minutes of sonication, each polymer was isolated by preparatory GPC and analyzed by ^{13}C NMR. It was found that both polymers **6** and **7** yield a single resonance at 174.2 ppm (Figure 2.9). The polymers appeared to yield the same products. This was confirmed by examination of mixtures. When 1:1 mixtures of products from sonication of LFPs **6** and **7** were measured in either $CDCl_3$ or CD_3OD, only a single peak was observed (Figure 2.10). Sonication of PEG under the same conditions yielded no detectable resonances in the carbonyl region.

In order to confirm that the major product after sonication of polymers **6** and **7** was due to the proposed chemistry, a small molecule model was prepared by reacting *trans*-1,2-

[3] In the 60 kDa PEG control polymer, the broken 30 kDa chains were observed to incorporate label much more so than PEG of lower MW. We speculate that this is due to a radical polymerization of the maleimide trap from the macroradicals resulting from chain scission. Radical polymerizations of unsaturated monomers initiated from the macroradicals formed upon chain scission has been previously reported. Price, G. *Advances in Sonochemistry* **1990**, *1*, 231.

Scheme 2.4. Preparation of Diels-Alder adduct **13.**

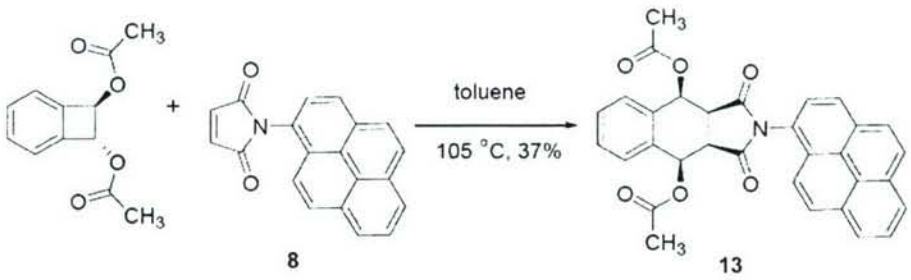

diacetoxybenzocyclobutene **10** and unlabeled pyrene trap **8** (Scheme 2.4). Diels-Alder adduct **13** was isolated in 37% yield.[4] A single crystal x-ray structure was obtained of this product, and was found to be the all-cis product which results from endo addition of the maleimide to the E,E-*o*QDM intermediate (Figure 5.11). The ^{13}C resonances of the imide carbonyl carbons in the small molecule model are consistent with the resonance from the major product in the mechanical reaction of polymers **6** and **7** (Figure 2.9). These results indicate that the observed adducts in the ultrasound reactions of LFPs **6** and **7** are indeed a result of ring opening, followed by a Diels-Alder cycloaddition.

In order to compare the products obtained under ultrasound conditions with those obtained under thermal conditions, maleimide trap **9** was reacted with polymer **6** in toluene at 105 °C and polymer **7** in xylenes at 140 °C (Arnold *et al.*, 1974). After isolation and ^{13}C analysis, the reaction products under thermal conditions were compared to the products obtained under ultrasound conditions. *trans*-LFP **6** reacted smoothly with maleimide **9** to give the same major product observed with polymer **6** and **7** under ultrasound conditions (Figure 2.9). However, in the thermal reaction a second minor peak was observed at 167 ppm, which results from thermal elimination of a carboxylic acid functional group in the Diels-Alder adduct to yield a N-pyrene-2,3-naphthimide ring system (Arnold *et al.*, 1974). The structure of this product was confirmed by single-crystal x-ray analysis (Figure 2.12).

The thermal reaction of polymer **7** did not yield any recognizable products. This is consistent with previous reports (Arnold *et al.*, 1974) and our own experience on small molecule model compounds that *cis*-1,2-diacetoxybenzocyclobutenes thermally degrade to a complex mixture. Observation of the product resulting from disrotatory ring opening suggests that ultrasound action is able to influence the specific pathway that a reactant follows. In effect, mechanical action forces the reactant down a thermally-disallowed disrotatory pathway (Figure 2.13). This is consistent with the computational studies, which suggested that stress would induce a disrotatory motion for the *cis* isomer, leading to the E,E-*o*QDM intermediate. Furthermore, this result suggests that the observed reaction is not a thermal process arising from flow-induced heat transfer because the thermal and ultrasound reaction
conditions yield different results.

In order to directly confirm that mechanical activation of the benzocyclobutene linker is occurring before polymer chain scission, polymer **6** was sonicated in the presence of maleimide trap **9**, yielding a mixture of broken and unbroken chains. The unbroken 40 kDa

[4] In this reaction, a 1:1 mixture of *cis* and *trans*-1,2-diacetoxy-1,2-dihydrobenzocyclobutenes was used. However, it has been previously shown that the *cis* isomer is unreactive in refluxing toluene (Arnold *et al.* 1974). Therefore, the isolated Diels-Alder adduct is due to the thermal ring opening of the *trans* isomer, followed by cycloaddition. A large amount of N-pyrene-2,3-naphthimide was also observed.

polymer was isolated by prep GPC (Figure 2.14a). It was found that the isolated 40 kDa material showed the characteristic UV increase of pyrene incorporation. Furthermore, ^{13}C analysis revealed that the Diels-Alder adduct was present in the uncleaved polymer strands (Figure 2.14b).

As further evidence of the chain length dependence described above, 4 kDa polymers **6** and **7** were subjected to ultrasound in the presence of ^{13}C labeled maleimide **9** (Figure 2.15). No Diels-Alder adduct was observed in either case. Furthermore, the polymers have low enough molecular weights that resonances corresponding to the benzocyclobutene linker can be observed at natural abundance, and are unchanged after subjection to mechanical conditions. These ^{13}C spectra reiterate the MW dependence of these linkers.

2.6 Conclusions

Mechanical deformation can be used to activate specific reaction pathways in mechanochemical triggers designed to harness the energy in a polymer under stress. Since activation of these triggers occurs before chain scission, we feel that they will be useful for the development of self-toughening polymeric materials. Upon activation, the oQDM intermediates could react with pendant dienophiles to form new crosslinks. The formation of crosslinks would be directly coupled and tailored to the stress field in a failing polymer. We also feel, with slight modification, that mechanochemical triggers could be useful for the stress-induced formation of new chromophores. The newly formed chromophores could then signal that some critical load has been reached, or perhaps signal the presence of microcracks. We expect that the procedures reported here will be generally useful for the development of utilizing mechanical energy to activate specific chemical pathways, and help shift the major focus of mechanochemical studies from bond-breaking to bond-making transformations.

2.7 Experimental Procedures

General Procedures: Unless otherwise stated, all starting materials and reagents were obtained from commercial suppliers and used without further purification. Methoxypoly(ethylene glycol) amine was purchased from Nektar Transforming Therapeutics (2, 5, 10, 20 kDa). PEG standards were purchased from Polymer Labs. 1-ethyl-3-(3-dimethylaminopropyl)-carbodiimide (EDC, 98%) was purchased from TSI. 1,4-^{13}C-maleic anhydride (99% isotope purity) was purchased from Cambridge Isotope Labs. 4-(dimethylamino) pyridine (DMAP, 99%), 1-aminopyrene (95%), and TBAF (1.0 M soln in THF) were purchased from Aldrich. $ZnBr_2$ was purchased from Strem, and 1,1,1-3,3,3-hexamethyldisilazide was purchased from Acros. N,N'-dicyclohexylcarbodiimide (DCC) was obtained from Avocado. Reagent grade ether was purchased from Malinckrodt and anhydrous methylene chloride was purchased from Acros and stored over 3Å molecular sieves. ACS grade acetonitrile was purchased from Aldrich and stored over 3Å molecular sieves.

Preparatory gel permeation chromatography (prep GPC) analyses were performed with a Waters 515 HPLC pump, a Waters 2487 UV detector, a 410 Differential Diffractometer, and a series of three Waters columns (19 X 300 mm, Ultrastyragel 10^4 Å THF, 10^2 Å THF, 500 Å THF) in a solution of THF (99.9%+, HPLC grade), inhibitor free. Analytical Gel permeation chromatography (GPC) analyses were performed with a Waters 515 HPLC pump, a Viscotek TDA Model 300 triple detector array, a Thermoseparations Trace Series AS100 autosampler, and series of three Viscotek Viscogel columns (7.8 X 300 mm, 2 GMHXL16141 and one G3000HXL16136) in a solution of 89% tetrahydrofuran and 10% methanol, with 1% triethylamine, at 30 °C. The GPC was calibrated with monodisperse polystyrene standards.

Ultrasound experiments were performed on a Vibra Cell 505 liquid processor with a 0.5 inch diameter solid probe from Sonics and Materials. The distance between the titanium tip and bottom of the Suslick cell was 1 cm. The Suslick cells were made by the School of Chemical Sciences' Glass Shop at the University of Illinois.

Flash chromatrography was conducted with silica gel 60 (230-400 mesh) from EM science. The ^{1}H and ^{13}C NMR specra were recorded on Varian Unity 500 MHz spectrometers in NMR laboratory, the residual solvent protons were used as an internal standard. Coupling constants (J) are reported in Hertz (Hz), and splitting patterns are designated as s (singlet), d (doublet), t (triplet), q (quartet), m (multiplet), and br (broad). Mass spec were obtained through the Mass Spectrometry Facility, SCS, University of Illinois.

***Trans*-1,2-bis[(3-carboxypropanoyl)oxy]-1,2-dihydrobenzocyclobutene 1**: To a 50 mL roundbottomed flask equipped with a magnetic stirrer and rubber stopper and purged with N_2 was added diketone **3** (0.148 g, 1.12 mmol) and methanol (33.7 mL). The resulting

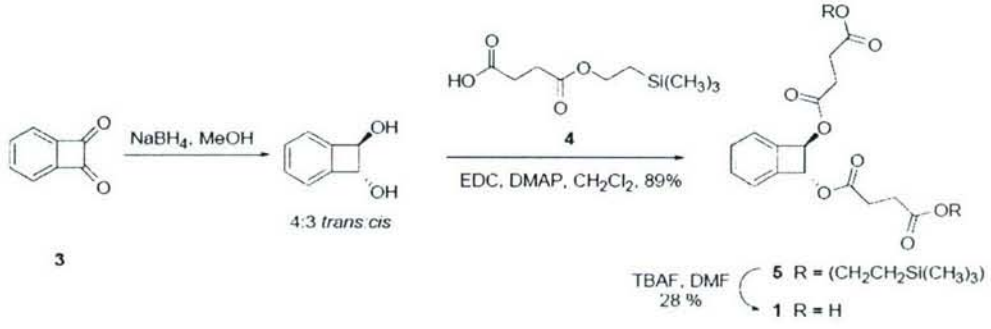

solution was cooled in an ice water bath, and $NaBH_4$ (85 mg, 2.25 mmol) was added in several portions. This was stirred for 30 min with cooling then quenched with acetone (2 mL) and the solvent was removed under vacuum at 0 °C. The residue was purified by flash chromatography at 4 °C in a cold box, using 3:2 hexane:EtOAc as the eluent. The later eluting spot was concentrated under vacuum at 0 °C, placed in a flask precooled in an ice bath and equipped with a magnetic stirrer and rubber stopper and charged with CH_2Cl_2 (2 mL). EDC (0.494 g, 2.58 mmol) and DMAP (27 mg, 0.225 mmol) were then added, followed by 4-(2-(trimethylsilyl)ethyl) ester butanoic acid **4** (0.49 g, 2.25 mmol). The solution was stirred with cooling and slowly warmed to room temperature. After 1.5 h the solvent was removed under vacuum. The residue was placed on a silica plug and the plug was eluted with 1:1 hexane:EtOAc. The filtrate was concentrated under vacuum, yielding an oil.

The residue obtained above was taken up in DMF (2-3 mL). TBAF in THF (1 M) was added in portions (0.5 mL) every 20 min until the reaction was complete by TLC. The

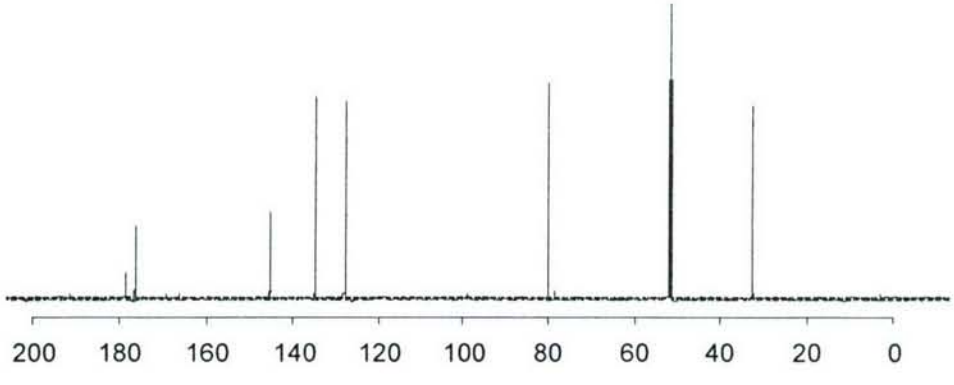

reaction was then partitioned between 1 M HCl and EtOAc (25 mL each). The layers were separated, and the aqueous layer was extracted with EtOAc (4 x 25 mL). The combined organics were dried over Na_2SO_4 and the solvent was removed under vacuum, yielding **1** (53 mg, 28 %) as a colorless oil: ^{1}H NMR (500 MHz, CD_3OD) δ 7.41 (dd, J = 2.9, 5.4 Hz, 2H), 7.30 (dd, J = 3.1, 5.6 Hz, 2H), 5.79 (s, 2H), 2.66 (m, 4H), 2.62 (m, 4H); ^{13}C NMR (CD_3OD, 125 MHz) _ 178.7, 176.4, 145.2, 134.6, 127.9, 80.1, 32.6, 32.5; ESI MS: calcd for $C_{16}H_{17}O_8$ $(M+H)^+$ 337.0923, found 337.0920.

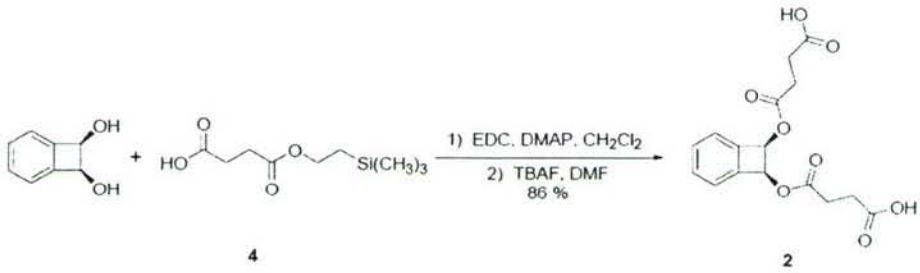

4 2

***Cis*-1,2-bis[(3-carboxypropanoyl)oxy]-1,2-dihydrobenzocyclobutene 2**: *Cis*-benzocyclobuten-1,2-diol (0.1774 g, 1.3 mmol) was suspended in CH_2Cl_2 (2 mL) in a 20 mL scintillation vial equipped with a magnetic stirrer and rubber stopper and purged with N_2. The suspension was cooled in an ice bath, then added was a solution of 4-(2-(trimethylsilyl)ethyl ester butanoic acid **4** (0.567 g, 2.6 mmol) in CH_2Cl_2 (0.6 mL), followed by EDC (0.569 g, 2.98 mmol) and 4-DMAP (31 mg, 0.25 mmol). The rubber stopper was replaced with a plastic screw cap and the solution was stirred and warmed to room temperature. After stirring for 10 h, the reaction was diluted with CH_2Cl_2 (5 mL) and washed with water (5 mL), 1 M HCl (5 mL), and satd $NaHCO_3$ (5 mL), then dried over Na_2SO_4. The solvent was removed under vacuum and the residue was used in the subsequent reaction without further purification.

Into a 20 mL scintillation vial equipped with a magnetic stirrer and plastic screw cap was added the residue obtained above and DMF (6.5 mL) A solution of TBAF in THF (3.9 mL of 1.0 M soln, 3.9 mmol) was then added, and the solution was stirred overnight. It was then partitioned between 1 M HCl (75 mL) and EtOAc (75 mL). The layers were separated and the aqueous layer was extracted with EtOAc (3 x 50 mL). The combined organics were washed with 1 M HCl and dried over Na_2SO_4. The solvent was removed under vacuum, and the yellow residue obtained was filtered through a silica plug, eluting with 6:3:1

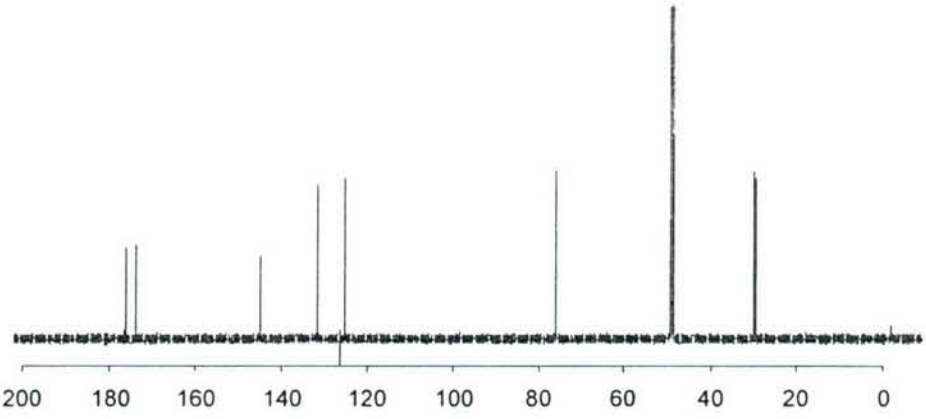

^{13}C NMR spectra for diacid **2** recorded as a solution in CD_3OD on a 125 MHz instrument.

hexane:EtOAC:AcOH. The filtrate was concentrated under vacuum, yielding **2** (0.381 g, 86%) as a white solid: ^{1}H NMR (500 MHz, CD_3OD) δ 7.42 (dd, J = 3.2, 5.5 Hz, 2H), 7.31 (dd, J = 3.2, 5.5 Hz, 2H), 6.22 (s, 2H), 4.90 (s, 2H), 2.68 (m, 4H), 2.61 (m, 4H); ^{13}C NMR (125 MHz, CD_3OD) δ 175.9, 173.7, 145.0, 131.2, 125.2, 75.8, 29.9, 29.6; ESI MS: calcd for $C_{16}H_{16}O_8Na$ $(M+Na)^+$ 359.0743, found 359.0730.

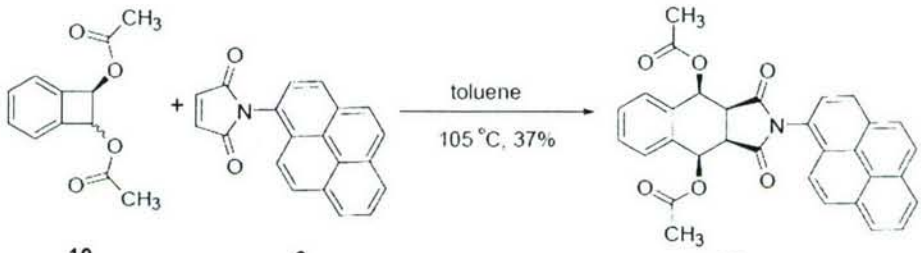

10 1:1 *trans*:*cis* **8** **13**

Diels-Alder adduct 13: A 1:1 mixture of *trans* and *cis*-1,2-diacetoxy-1,2-dihydrobenzocyclobutene (0.11 g, 0.249 mmol of *trans* isomer) was placed into 15 mL round bottom flask equipped with a magnetic stirrer and reflux condenser. Maleimide **8** (70.4 mg, 0.237 mmol) was added, followed by toluene (7.8 mL). The resulting solution was warmed to 105 °C and stirred for 48h. The solvent was removed under vacuum and the residue was purified by column chromatography (3:1 chloroform:diethyl ether), yielding **13** (45.6 mg, 37 %) as a red solid: ^{1}H NMR ($CDCl_3$, 500 MHz) δ 8.26 (t, J = 8.4 Hz, 2H), 8.19 (d, J = 7.5 Hz, 1H), 8.15 (d, J = 9.0 Hz, 1H), 8.10 (d, J = 8.8 Hz, 1H), 8.05 (t, J = 7.9 Hz, 1H), 7.95 (d, J = 9 Hz, 1H), 7.82 (d, J = 7.7 Hz, 1H), 7.74 (dd, J = 3.7, 5.3 Hz, 2H), 7.60 (br s, 1H), 7.54 (dd, J = 3.4, 5.4 Hz, 2H), 6.52 (app q, J = 1.8 Hz, 2H), 3.92 (app q, J = 2.2 Hz, 2H), 2.20 (s, 6H); ^{13}C NMR ($CDCl_3$, 125 MHz) _ 174.2, 169.7, 133.8, 132.5, 131.2, 130.9, 130.0, 129.9, 129.8, 129.0, 128.9, 127.8, 127.3, 126.7, 126.5, 126.0, 125.8, 125.5, 124.9, 124.6, 121.3, 67.5, 43.4, 21.2; EI MS: calc'd for $C_{32}H_{23}NO_6$ 517.1525, found 517.1523. TLC analysis indicated that the *cis* isomer was unconsumed during the reaction, consistent with previous literature reports that this isomer is unreactive in boiling toluene (Pouzair *et al.*, 1984).

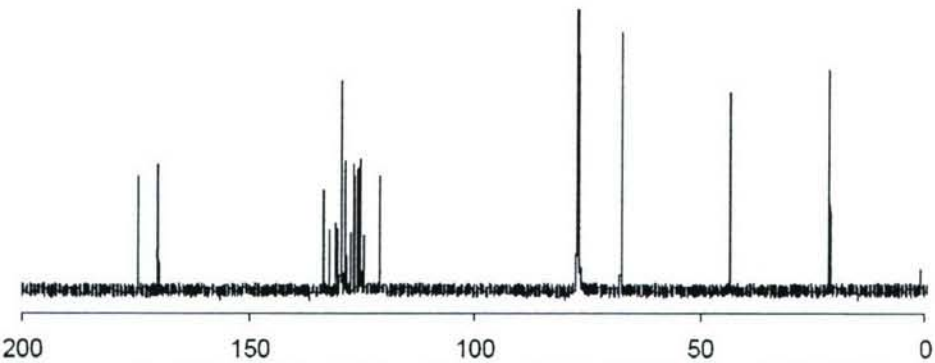

^{13}C NMR spectra for Diels-Alder Adduct **13** recorded in $CDCl_3$ on a 125 MHz instrument.

Synthesis of Center Link-Functionalized Polymers. General Procedure: α-methoxy-ω-amino poly(ethylene glycol) (mPEG-NH_2, 2 equiv), diacid linker (1 equiv), N,N'-dicyclohexylcarbodiimide (DCC, 5 equiv) and DMAP, (1 equiv) were dissolved in a small amount of CH_2Cl_2 (approximately 1.5 mL per 1 g of polymer) and stirred at room temp for 24 h in the dark. The dicyclohexylisourea byproduct (DCU) was removed by filtration through a cotton plug. The filtrate was then slowly precipitated into 200-times its volume of ether. After cooling of the ether to -20 °C, the polymer was collected by filtration through a fritted funnel, then washed with ether and dried under vacuum. Typical conversions from the starting polymer to the link-functionalized polymer with a MW double the starting value ranged from 60-90%.

Set-up of the ultrasound apparatus: For each ultrasound experiment, a solution of the polymer was placed in a Suslick cell (a flat-bottomed, glass vessel containing three side arms) that was inserted into a collar, and screwed onto the transducer. A thermocouple and an argon line were threaded through the septa on two of the Suslick cell side arms and placed in contact with the solution, ensuring that they did not touch the probe. The third side arm of the cell contained a septum that was threaded with a needle. Argon was bubbled through the solution for 30 min prior to each experiment as well as during the experiment. The entire system was placed in an ice bath to maintain a temperature of 0-9 °C throughout sonication.

Calibration of the sonication equipment: Calorimetry was used to calibrate the ultrasonic intensity produced by the probe. A small dewar was filled with exactly 250 mL of Millipore water and the probe was submerged approximately 0.5 inches into the water. The exact height was marked for reproducibility. A thermocouple was then introduced into the water and the temperature was allowed to stabilize. The amplitude on the processor was set to 21%, the temperature was recorded at 0 sec, and sonication was started. The temperature of the water was recorded every 15 s for 3 min, and these values were plotted against time to determine Δ temperature/Δ time by the slope of the line. This procedure was repeated for amplitudes of 30, 40, 50, 60, 70, and 80%.

The heat due to cavitation in J/s, or W, was determined from the following equation: q = specific heat ($Jg^{-1}\,°C^{-1}$) X mass (g) X Δ temperature/Δ time (°C/s) where the specific heat of water = 4.179 $Jg^{-1}\,°C^{-1}$, the mass of water = 250 g, and Δ temperature/Δ time = the slope of the line. The resulting value, q, was divided by the surface area of the horn tip (1.27 cm^2 for a 5 inch tip) to find W/cm^2. Finally, the power produced was plotted against the percentage of amplitude to generate the calibration curves.

General procedures for sonication of polymers: A solution was made of 0.75 mg/mL polymer in acetonitrile (~19 μM for 40 kDa polymers). To this solution was added maleimide trap **8** or **9**[5] (2.75 mg/mL). Approximately 12 mL of this solution was introduced into a Suslick cell. A thermocouple and an argon line were threaded through the septa on two of the Suslick cell side arms and placed in contact with the solution, ensuring that they did not touch the probe. The third side arm of the cell contained a septum. The cell was then wrapped in aluminum foil to exclude light. Argon was bubbled through the solution for 30 min prior to each experiment as well as during the experiment. The entire

[5] For the studies reported here, typically the trap was not purified any further than described by Reddy *et al* (1998). On occasion, the use of maleimide **8** after recrystallization from toluene resulted in significant baseline drift in the UV signal. The baseline drift did not show up in the RI curves. The drift was attributed to small amounts of a radical polymerization initiated by the ultrasound conditions. The polymerization of unsaturated monomers initiated by ultrasound has been previously described. See, for example, Lindström, O.; Lamm, O.J. *J. Phys. Coll. Chem.* **1951**, *55*, 1139. The addition of a radical inhibitor, such as BHT, was found to minimize this baseline drift. Control experiments comparing the UV/RI ratio with and without added BHT show that the presence of a radical inhibitor has no effect on the measured UV/RI ratio for 40 kDa LFPs **6** or **7**, or for 43 kDa PEG.

system was placed in an ice bath to maintain a temperature of 6-9 °C throughout sonication. The sample was then sonicated (pulsed on 0.5 s, off 1.0 s, 8.73 W/cm^2) for 45 min total time (15 min sonication time). After sonication, the solvent was removed and the polymer sample was isolated by prep GPC.

Determination of UV/RI Ratios: After isolation of the polymer, a GPC trace was recorded on a GPC equipped with three Waters Ultrastyragel prep GPC columns (10^4 Å, 10^3 Å, and 500 Å) in THF, a Waters 2487 UV detector, and a Waters 410 RI detector. The UV detector sensitivity was set at 4.00 aufs, and the absorption for all experiments was monitored at 345 nm. The RI sensitivity was set at 8, and the temperature at the detector was thermostated between 31.9-32.5 °C. After the trace was recorded, the area under the UV and RI curves for unbroken chains was measured using triSEC software (version 3.0, revision B.00.05). The baseline and integration limits were set to include only the unbroken chains using the RI trace. The UV area was then measured without changing the position of the integration limits. Typically, the baseline in the UV trace was fixed to include only the area included in the integration limits.

^{13}C NMR Experiments: For ^{13}C labeling experiments, the polymer of interest was sonicated as above with the ^{13}C labeled maleimide trap. The polymer from two such runs was isolated by prep GPC and combined in an NMR tube with the appropriate solvent. The spectra were recorded on a 500 MHz instrument with about 10-15 mg of polymer dissolved in 0.5 mL of solvent with between 15,000-17,000 acquisitions.

2.8 References

Segure, J.L.; Martin, N. *Chem. Rev.* **1999**, *99*, 3199.

Huisgen, R.; Seidl, H. *Tetrahedron Lett.* **1964**, 3381.

Sakai, S. *J. Phys. Chem. A* **2000**, *104*, 11615.

Roth, W.R.; Rekowski, V.; Börner, S.; Quast, M. *Liebigs Ann.* **1996**, 409.

Kirmse, W.; Rondan, N.G.; Houk, K.N. *J. Am. Chem. Soc.* **1984**, *106*, 7989.

Rondan, N.G.; Houk, K.N. *J. Am. Chem. Soc.* **1985**, *107*, 2099.

Spellmeyer, D.C.; Houk, K.N.; *J. Am. Chem. Soc.* **1988**, *110*, 3412 and references therein.

Jefford, C.W.; Bernardinelli, G.; Wang, Y.; Spellmeyer, D.C.; Buda, A.; Houk, K.N. *J. Am. Chem. Soc.* **1992**, *114*, 1157.

Mariet, N.; Pellissier, H.; Parrian, J-L.; Santelli, M.; *Tetrahedron* **2004**, *60*, 2829.

Errede, L. A. *J. Am. Chem. Soc.* **1961**, *83*, 949.

Beyer, M.K. *J. Chem. Phys.* **2000**, *112*, 7307-7312.

Jefford, C.W.; Bernardinelli,G.; Wang,Y.; Spellmeyer, D.C.; Buda, A.; Houk, K.N. *J. Am. Chem. Soc.* **1992**, *114*, 1157.

Kirmase, W.; Rondan, N.G.; Houk, K.N. *J. Am. Chem. Soc.* **1984**, *106*, 7989.

South, M.S., Lesbeskind, L.S. *J. Org. Chem.* **1982**, *47*, 3815-3821.

Allen, J.G.; Hentemann, Martin F.; Danishefsky, S.J. *J. Am. Chem. Soc.* **2000**, *122*, 571-575.

Nozaki, H.; Noyori, R.; Kozaki, N. *Tetrahedron* **1964**, *20*, 641.

Pouzair, V.; Drasar, P.; Cerny, I.; Havel, M. **1984**, *14*, 501.

Berkowski, K.L.; Potisek, S.L.; Hickenboth, C.R.; Moore, J.S. *Macromolecules* **2005**, *38*, 8975.

Reddy, P.Y., Kondo, S., Fujita, S., Toru, T. *Synthesis* **1998**, 999-1002.

Arnold, B.J.; Sammes, P.G.; Wallace, T.W. *J. Chem. Soc. Perkins Trans. I.* **1974**, 415.

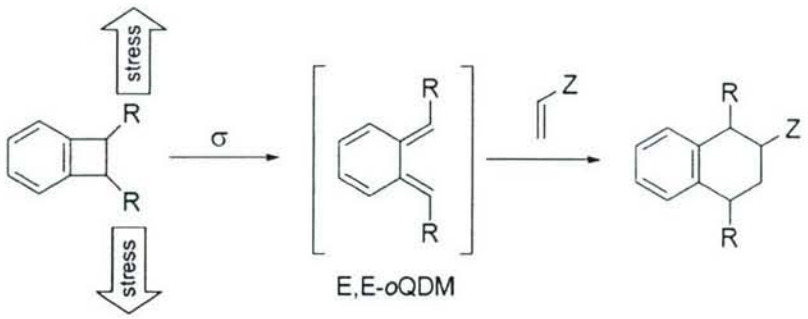

Figure 2.1. In benzocyclobutene-based mechanochemical triggers, it is proposed that stress can promote electrocyclic ring opening to a potent *o*QDM diene. This highly-reactive intermediate can react with pendant dienophiles in the polymer backbone to create new carbon-carbon bonds in the region of stress.

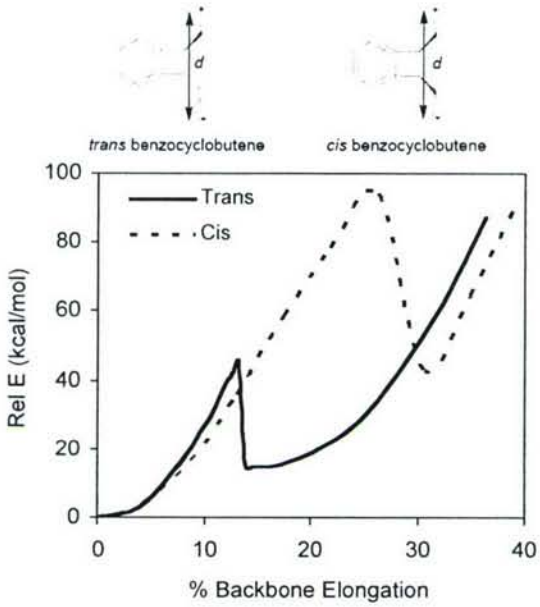

Figure 2.2. Plot of relative energy vs % backbone elongation for *trans* and *cis* 1,2-diethylbenzocyclobutene. The backbone elongation is defined as the % elongation of distance *d* between the methyl carbons (marked *) of *trans* and *cis* diethylbenzocyclobutene, relative to *d* in the ground state. Energies were calculated at the DFT B3LYP/6-31G* level.

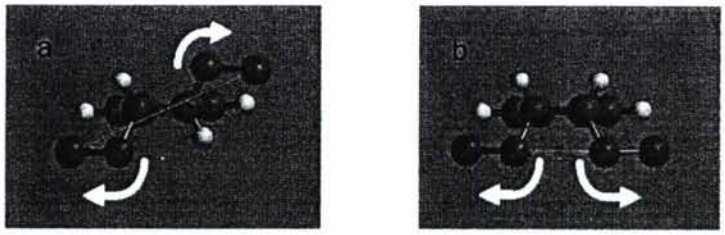

Figure 2.3. The difference between the efficiency of stress activation between *trans* and *cis* benzocyclobutene has been attributed to effective torque. a) In *trans*-benzocyclobutenes, elongational stress applied along the red vector induces a conrotatory motion of the substituents to yield an E,E-*o*QDM intermediate. b) In *cis*-benzocyclobutenes, elongational stress applied along the red vector induces a disrotatory motion of the substituents, leading to an E,E-*o*QDM intermediate.

Table 2.1. Comparison of calculated and experimental energies of activation for ring opening of disubstituted cyclobutenes.

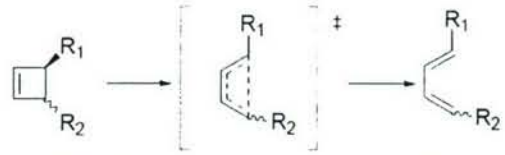

R_1	R_2	Calc'd E_A[a](kcal/mol)	Experimental E_A (kcal/mol)[b]	% error
Cl	*cis*-Cl	36.4	35.6	2.2
Cl	*trans*-Cl	26.3	25.7	2.3
OCH_3	*cis*-OCH_3	25.9	28.8	10

[a] E_As calculated at the DFT B3LYP/6-31G* level using Spartan '04.

[b] Ref 5.

Table 2.2. Calculated activation energies for ring opening of *trans*-disubstituted benzocyclobutenes.

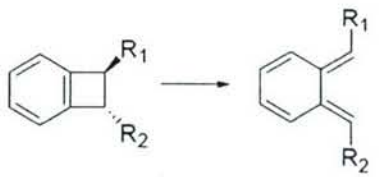

R_1	R_2	Calc'd E_a[1] (kcal/mol)
$NHCH_3$	$NHCH_3$	20.5
OCH_3	OCH_3	24.6
$NHCH_3$	CH_2CH_3	27.0
OAc	OAc	29.4
OCH_3	CH_2CH_3	30.9

[1] Calculated at the B3LYP/6-31* level using Spartan '04, Wavefunction, Inc.

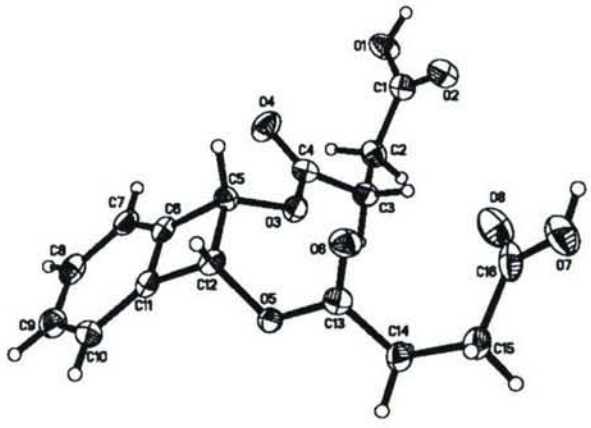

Figure 2.4. ORTEP thermal ellipsoid diagram at the 50% probability for *cis*-benzocyclobutene linker **2**.

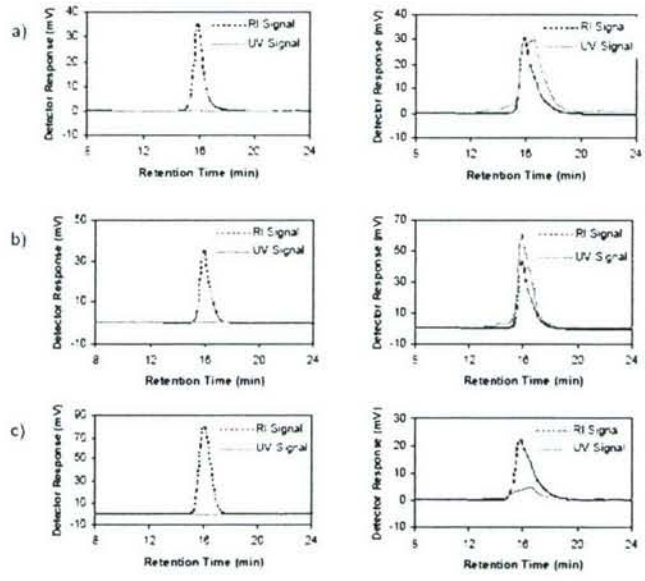

Figure 2.5. GPC traces of a) LFP **6** before (left) and after (right) sonication, b) LFP **7** before (left) and after (right) sonication, c) 43 kDa PEG control before (left) and after (right) sonication. All polymers were sonicated as a solution in acetonitrile (0.75 mg/mL) containing N-pyrene maleimide trap (2.75 mg/mL, ca 500 equiv) at a frequency of 20 kHz and a power of 8.7 W/cm,^{2} under argon and at 5-10 °C, then the polymer was purified by preparatory GPC.

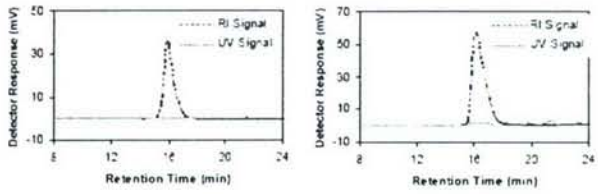

Figure 2.6. GPC traces before (left) and after (right) LFP **7** was subjected to the testing conditions, except ultrasound was omitted. LFP **7** was dissolved in acetonitrile (0.75 mg/mL) containing N-pyrene maleimide trap (2.75 mg/mL, ca 500 equiv), purged with argon and cooled to ca 1 °C. After standing for 45 min, the solvent was removed and the polymer was purified by preparatory GPC.

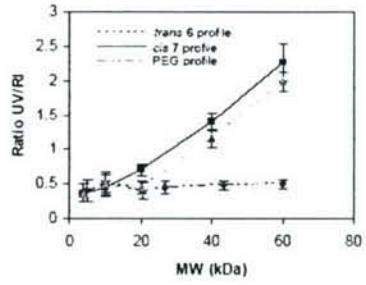

Figure 2.7. Plot of UV/RI signal ratio vs MW for sonicated LFPs containing *trans* and *cis* benzocyclobutene linkers, and also for PEG control. Only unbroken chains were considered. Error bars represent standard deviations of 3-6 measured values. All polymers were sonicated as a solution in acetonitrile (0.75 mg/mL) containing N-pyrene maleimide trap (2.75 mg/mL, ca 500 equiv) at a frequency of 20 kHz and a power of 8.7 W/cm,^{2} under argon and at 5-10 °C, then purified by preparatory GPC

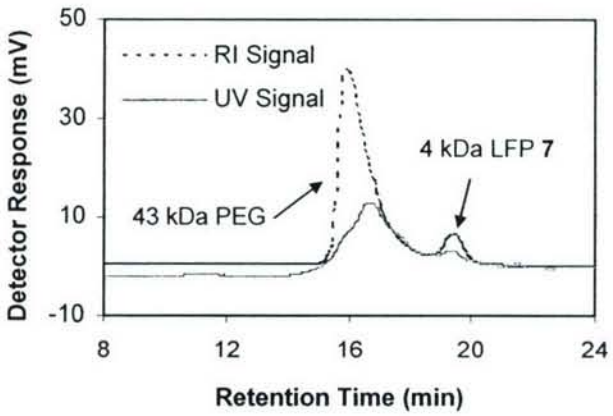

Figure 2.8. GPC trace after sonication of a 1:1 mol ratio mixture of 43 kDa unfunctionalized PEG and 4 kDa LFP **7**. The polymers were sonicated as a solution in acetonitrile (0.75 mg/mL) containing N-pyrene maleimide trap (2.75 mg/mL, ca 500 equiv) at a frequency of 20 kHz and a power of 8.7 W/cm,^{2} under argon and at 5-10 °C, then purified by preparatory GPC.

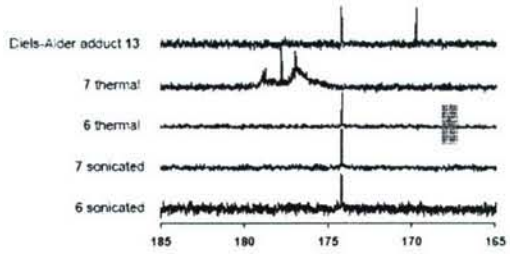

Figure 2.9. ^{13}C NMR spectrum comparing the products of polymers **6** and **7** with ^{13}C labeled maleimide trap **9** formed under thermal and ultrasound conditions, and small molecule Diels-Alder adduct **13**. The resonance assigned to the imide carbonyl in adduct **13** (shaded red) is consistent with the resonance observed in the mechanical reactions of polymers **6** and **7**, and in the major product by sonication of **6**. No such response is observed in the thermal reaction of polymer **7**. The peak shaded green has been assigned to the thermal elimination product, and the peak shaded blue has been assigned as the ester carbonyl in small molecule **13** at natural abundance. All spectra were recorded as solutions (ca 20 mg/mL) in $CDCl_3$ on a 125 MHz instrument.

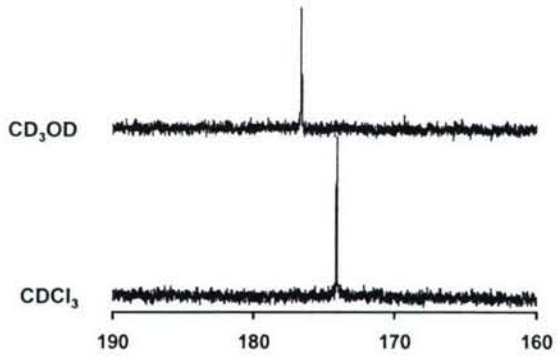

Figure 2.10. ^{13}C NMR spectra of a 1:1 mixture of sonicated LFPs **6** and **7** in $CDCl_3$ and CD_3OD. Only a single peak is observed in each solvent. This is consistent with both *trans* and *cis* benzocyclobutene linkers yielding the same products after sonication. The spectra were recorded on a 125 MHz instrument.

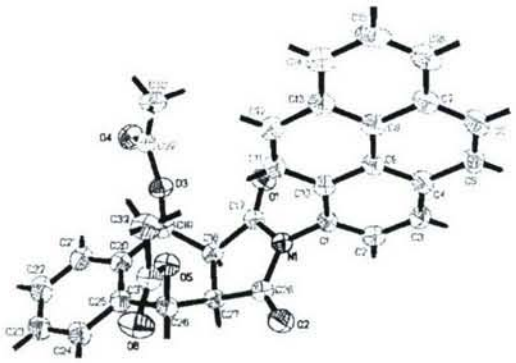

Figure 2.11. ORTEP thermal ellipsoid diagram at the 50% probability for Diels-Alder adduct **13**.

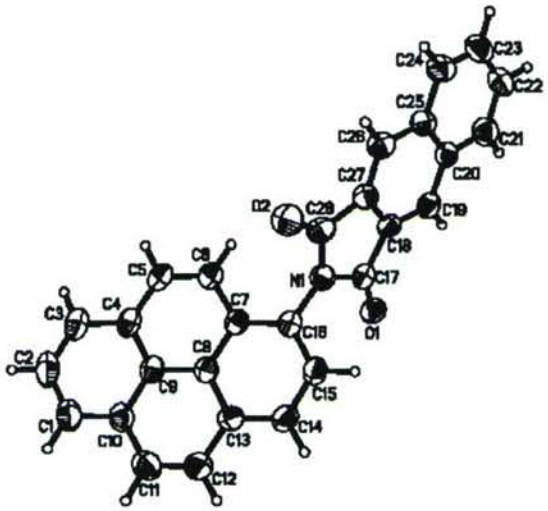

Figure 2.12. ORTEP thermal ellipsoid diagram at the 50% probability for N-pyrene-2,3-naphthimide.

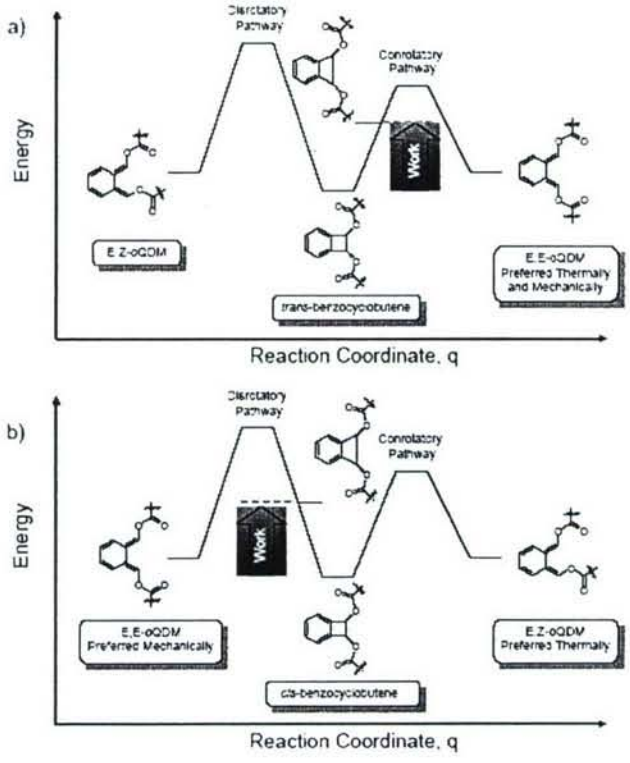

Figure 2.13. A schematic diagram of the potential energy surface and the changes that result from an external stress field. a) In *trans*-benzocyclobutenes, stress is able to promote a formal conrotatory ring opening to the E,E-*o*QDM intermediate. The stress-induced conrotatory deformations for this pathway are better aligned with the motions of atoms for conrotatory ring opening. b). In *cis*-benzocyclobutenes, stress is able to promote a formal disrotatory ring opening to the E,E-*o*QDM intermediate, even though it is the higher energy ring opening pathway.

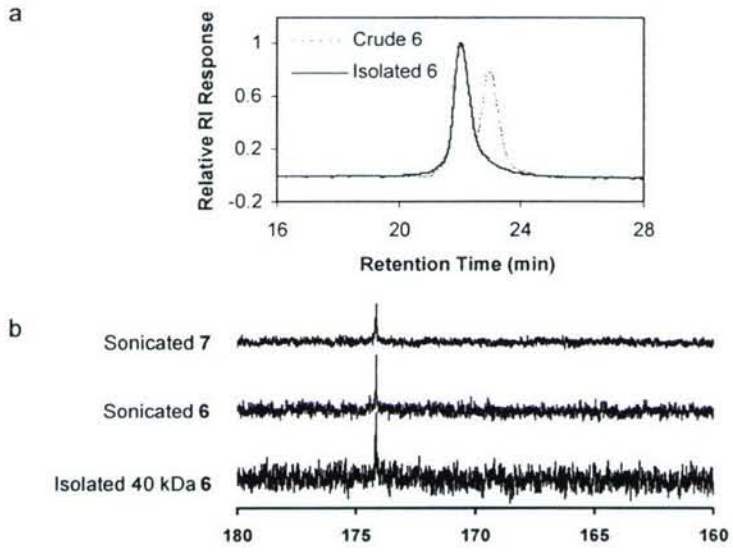

Figure 2.14. a) Analytical GPC trace showing sonicated LFP **6** after sonication, as a mixture of 40 kDa unbroken chains and 20 kDa broken chains, and after isolation of unbroken chains by prep GPC. b) ^{13}C NMR spectra comparing isolated unbroken 40 kDa polymer **6** after sonication to crude LFP **6** and LFP **7** after sonication. The Diels-Alder adduct is still observed after isolation, suggesting that mechanochemical activation of benzocyclobutene is occurring before polymer chain scission.

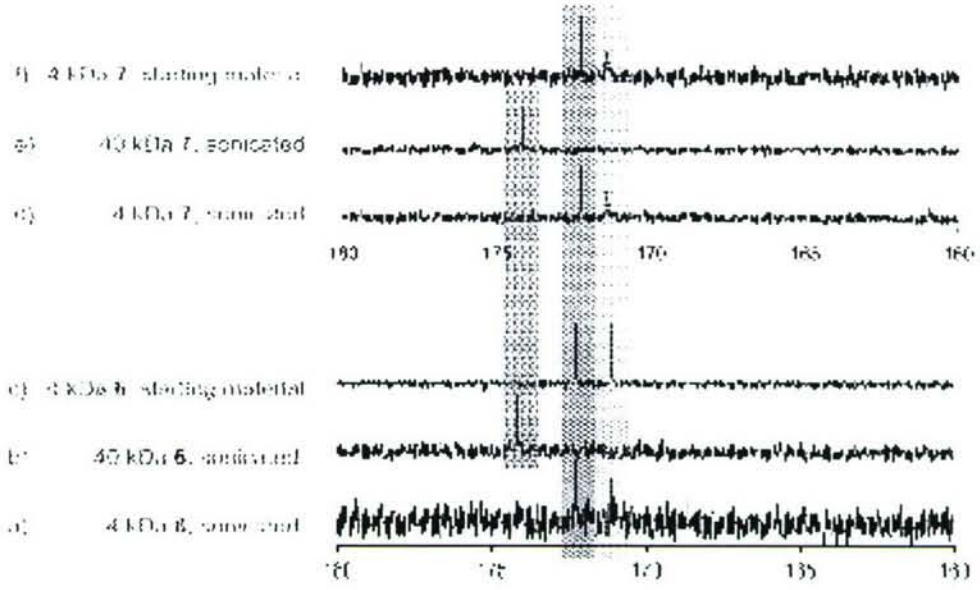

Figure 2.15. Portions of the ^{13}C NMR spectra showing the effect of chain length on the formation of the Diels-Alder adducts. No peaks corresponding to Diels-Alder adducts were observed in 4 kDa polymers containing linkers **1** (a) and **2** (d). Furthermore, the ^{13}C resonances of the benzocyclobutene linkers corresponding to the amide carbonyl (shaded blue) and ester carbonyl (shaded green) at natural abundance can be observed, and appear to be unchanged after mechanical treatment. With 40 kDa polymers containing linker **1** (b) and linker **2** (e), the Diels-Alder adduct is observed (shaded red). All NMR spectra were recorded as solutions in $CDCl_3$ (ca 20 mg/mL) on a 125 MHz instrument.

Figure 2.16. GPC chromatograms taken before (left) and after (right) sonication for 4kDa, 10kDa, 20kDa, and 60 kDa LFPs, and for 5kDa, 10kDa, 20kDa, 26kDa and 60kDa PEG control.

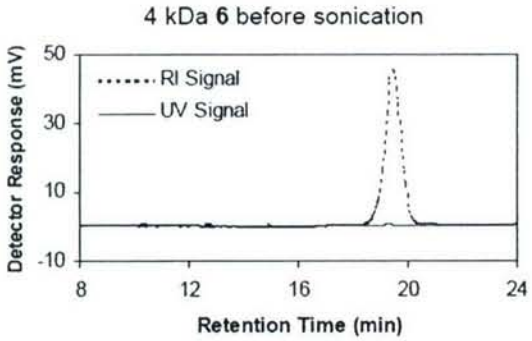

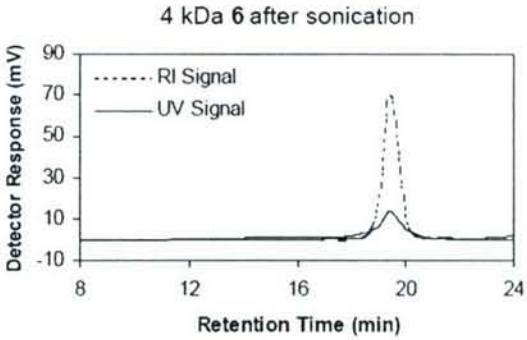

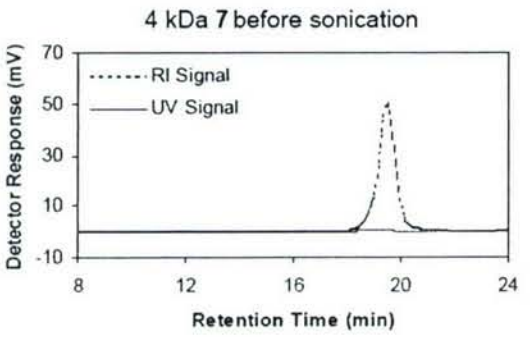

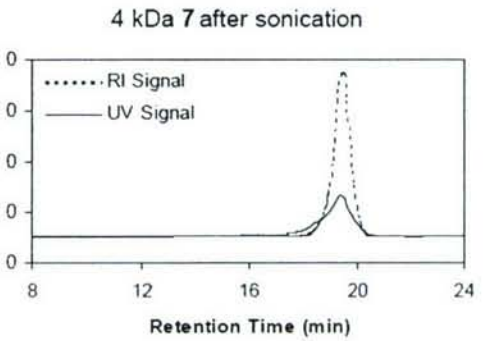

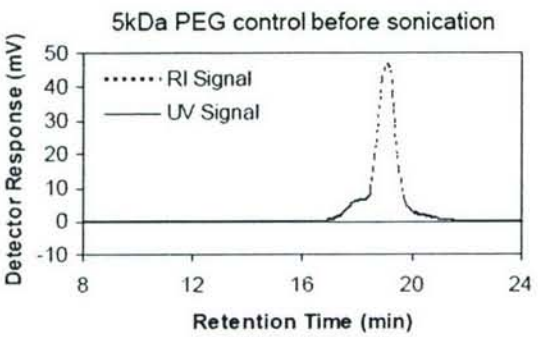

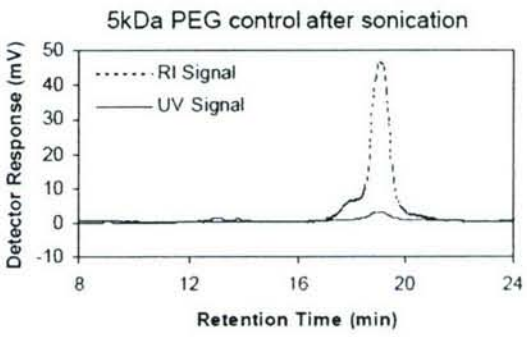

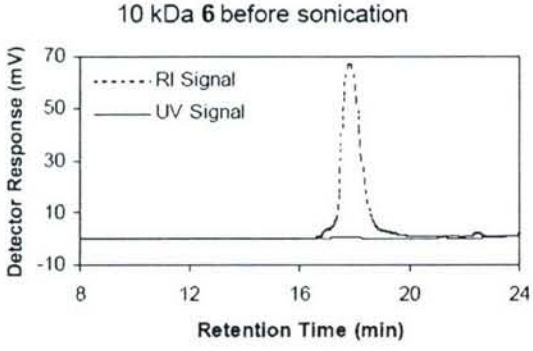
10 kDa 6 before sonication
RI Signal
UV Signal
Detector Response (mV)
70
50
30
10
-10
8
12
16
20
24
Retention Time (min)

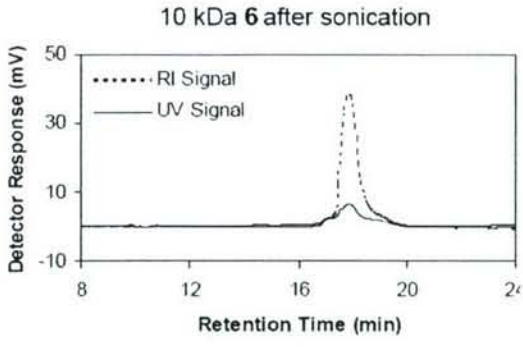
10 kDa 6 after sonication
RI Signal
UV Signal
Detector Response (mV)
50
30
10
-10
8
12
16
20
Retention Time (min)

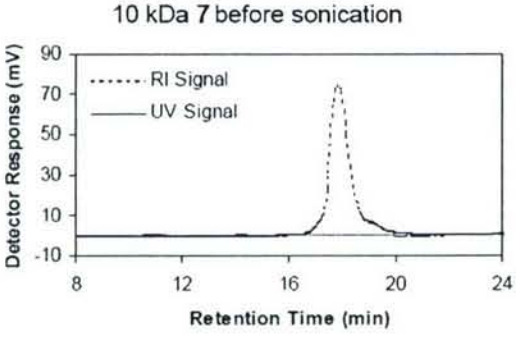
10 kDa 7 before sonication
RI Signal
UV Signal
Detector Response (mV)
90
70
50
30
10
-10
8
12
16
20
24
Retention Time (min)

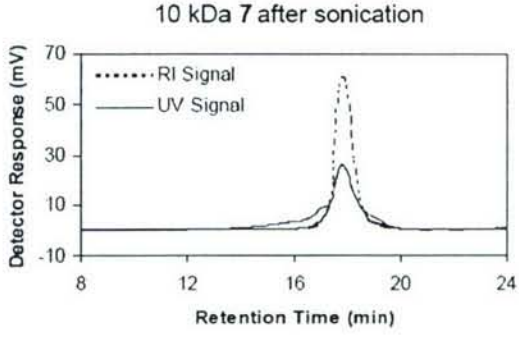
10 kDa 7 after sonication
RI Signal
UV Signal
Detector Response (mV)
70
50
30
10
-10
8
12
16
20
24
Retention Time (min)

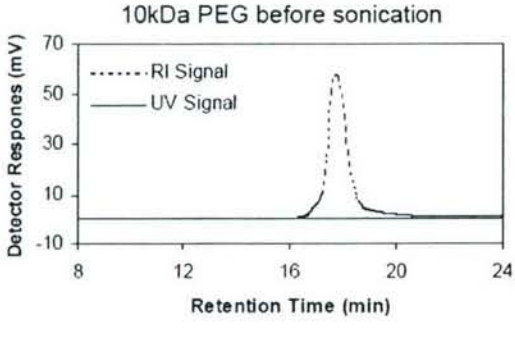
10kDa PEG before sonication
RI Signal
UV Signal
Detector Respones (mV)
70
50
30
10
-10
8
12
16
20
24
Retention Time (min)

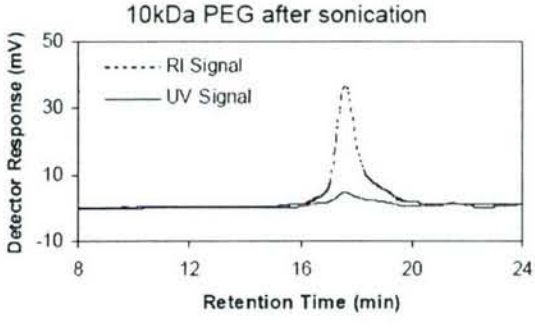
10kDa PEG after sonication
RI Signal
UV Signal
Detector Response (mV)
50
30
10
-10
8
12
16
20
24
Retention Time (min)

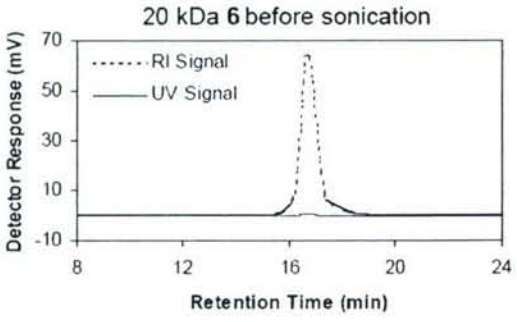
20 kDa 6 before sonication
RI Signal
UV Signal
Detector Response (mV)
70
50
30
10
-10
8
12
16
20
24
Retention Time (min)

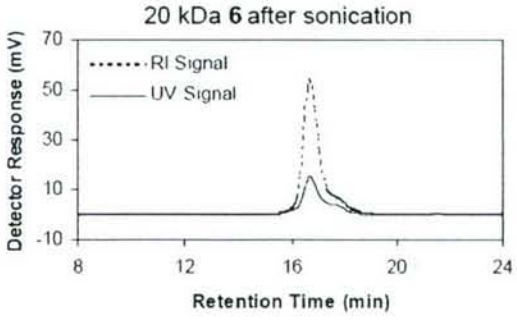
20 kDa 6 after sonication
RI Signal
UV Signal
Detector Response (mV)
70
50
30
10
-10
8
12
16
20
24
Retention Time (min)

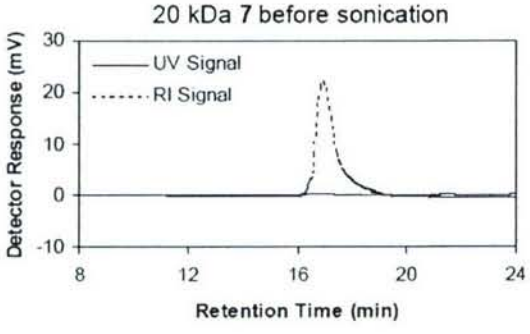
20 kDa 7 before sonication
UV Signal
RI Signal
Detector Response (mV)
30
20
10
0
-10
8
12
16
20
24
Retention Time (min)

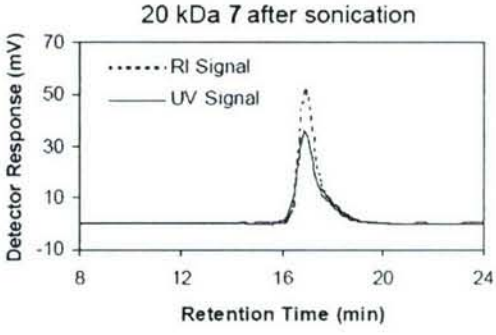
20 kDa 7 after sonication
RI Signal
UV Signal
Detector Response (mV)
70
50
30
10
-10
8
12
16
20
24
Retention Time (min)

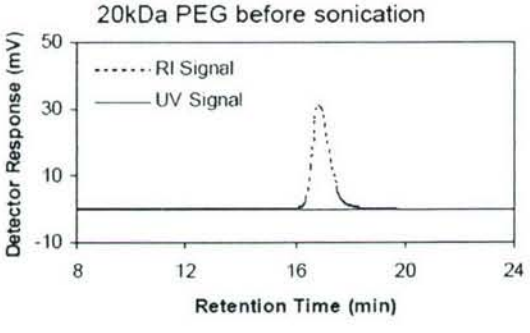
20kDa PEG before sonication
RI Signal
UV Signal
Detector Response (mV)
50
30
10
-10
8
12
16
20
24
Retention Time (min)

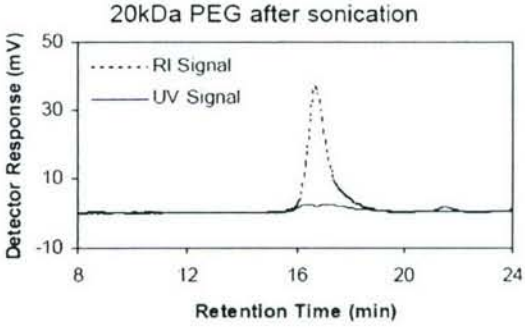
20kDa PEG after sonication
RI Signal
UV Signal
Detector Response (mV)
50
30
10
-10
8
12
16
20
24
Retention Time (min)

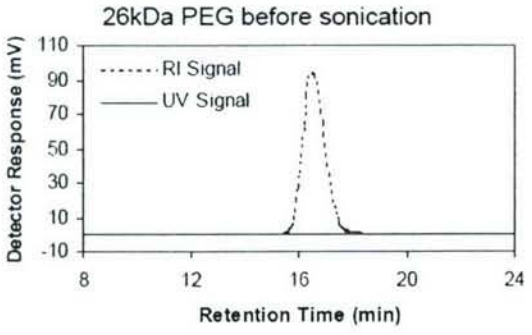
26kDa PEG before sonication
RI Signal
UV Signal
Detector Response (mV)
Retention Time (min)

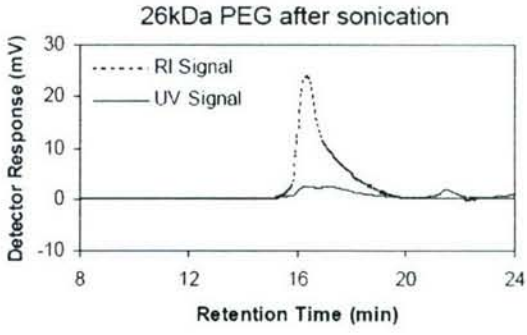
26kDa PEG after sonication
RI Signal
UV Signal
Detector Response (mV)
Retention Time (min)

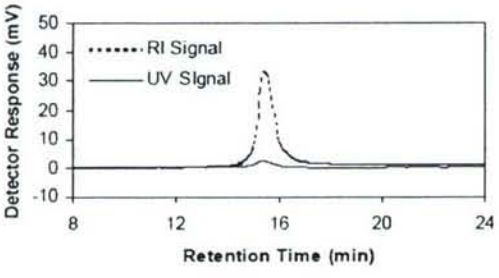
60 kDa 6 before sonication
RI Signal
UV SIgnal
Detector Response (mV)
Retention Time (min)

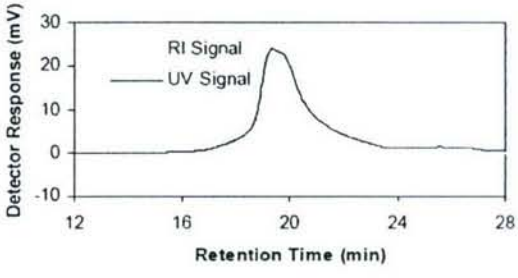
60 kDa 6 after sonication
RI Signal
UV Signal
Detector Response (mV)
Retention Time (min)

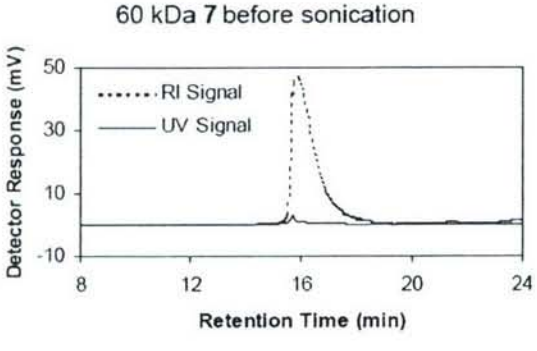
60 kDa 7 before sonication
RI Signal
UV Signal
Detector Response (mV)
Retention Time (min)

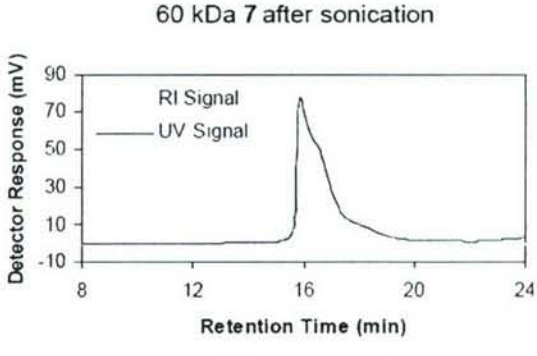
60 kDa 7 after sonication
RI Signal
UV Signal
Detector Response (mV)
Retention Time (min)

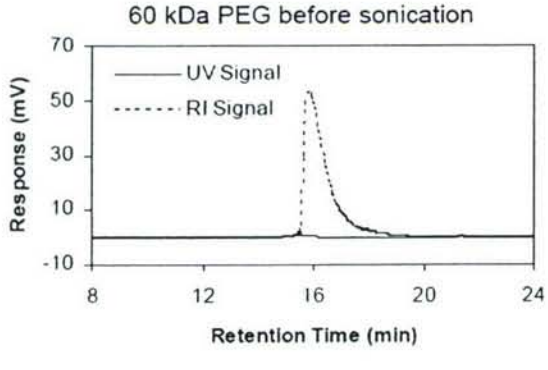
60 kDa PEG before sonication
UV Signal
RI Signal
Response (mV)
Retention Time (min)

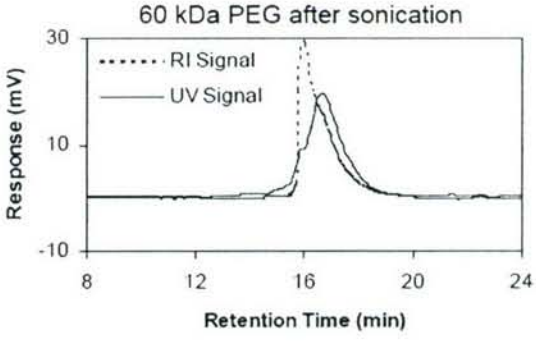
60 kDa PEG after sonication
RI Signal
UV Signal
Response (mV)
Retention Time (min)

PERSONNEL SUPPORTED

Faculty: S. White, J. Moore, N. Sottos

Students: J. Rule (summer, '03), D. Therriault (PhD graduate, Dec. 2003), J. Kamphaus, C. Hickenboth (PhD graduate, March, 2006)

PUBLICATIONS

A.S. Jones, J. Rule, J.S. Moore, S.R. White, N.R. Sottos, "Catalyst morphology and dissolution kinetics for self-healing polymers," *Chemistry of Materials*, 18, **2006**, pp. 1312-1317.

E.N. Brown, S.R. White, and N. R. Sottos, "Fatigue crack propagation in microcapsule toughened epoxy," *Journal of Materials Science*, 41, **2006**, pp. 6266-6273.

E.N. Brown, S.R. White, and N.R. Sottos, "Retardation and repair of fatigue cracks in a microcapsule toughened epoxy composite–Part 2: In situ self-healing," *Composites Science and Technology*, Special Anniversary Issue, 65, **2005**, pp. 2474-2480.

E.N. Brown, S.R. White, and N.R. Sottos, "Retardation and repair of fatigue cracks in a microcapsule toughened epoxy composite–Part 1: Manual infiltration," *Composites Science and Technology*, Special Anniversary Issue, 65, **2005**, pp. 2466-2473.

J.S. Moore, J.D. Rule, C. Hickenboth, N.R. Sottos, S.R. White, "Advances in self-healing polymers," *Abstracts of Papers of the American Chemical Society*, 229(2), **2005**, p. U903.

J.D. Rule, N.R. Sottos, S.R. White, J.S. Moore, "The chemistry of self-healing polymers," *Education in Chemistry*, 42(5), **2005**, pp. 130-132.

J.D. Rule, J.S. Moore, "Polymerizations initiated by diradicals from cycloaromatization reactions" *Macromolecules*, 38, **2005**, pp. 7266-7273.

J.D. Rule, E.N. Brown, N.R. Sottos, S.R. White, J.S. Moore, "Wax-protected catalyst microspheres for efficient self-healing materials," *Advanced Materials*, **2005**, 17(2), pp. 205-208.

K. Toohey, S.R. White, N.R. Sottos, "Self-healing polymer coatings," *Proceedings of the SEM Annual Meeting on Experimental and Applied Mechanics*, Society for Experimental Mechanics, CD-ROM, Portland, OR, June 6-9, **2005**.

S.R. White, S. Maiti, A.S. Jones, E.N. Brown, N.R. Sottos, and P.H. Geubelle, "Fatigue of self-healing polymers: multiscale analysis and experiments," *11th International Congress on Fracture*, Paper No. 5414, March 20-25, **2005**, Turin, Italy.

J.D. Rule, J.S. Moore, "Bergman cyclization in the presence of monomer: A systematic study of polymerization and competing reactions," *Abstracts of Papers of the American Chemical Society*, 228(2), **2004**, p. U371.

J.S. Moore, J.D. Rule, S.R. Wilson, "Diradical-initiated polymerization via Bergman cyclization," *Abstracts of Papers of the American Chemical Society*, 227(2), **2004**, p. U421.

E.N. Brown, S.R. White and N.R. Sottos, "Microcapsule induced toughening in a self-healing polymer composite," *Journal of Materials Science*, 39, **2004**, pp. 1703-1710.

S.R. White, N.R. Sottos, K.S. Toohey, "Autonomic healing of polymer coatings," *European Coatings Conference – Smart Coatings III*, CD-ROM, June 7-9, **2004**, Berlin, Germany.

S.R. White, N.R. Sottos, J.S. Moore, E.N. Brown, A.S. Jones, J. Rule, "Autonomic healing of polymers and composites," *21st International Congress of Theoretical and Applied Mechanics (ICTAM),* Paper No. 11684, August 15-21, **2004**, Warsaw Poland.

E.N. Brown, N.R. Sottos, S.R. White, "Fatigue crack arrest in a self-healing polymer composite," *Proceedings of SEM Annual Conference on Experimental and Applied Mechanics*, Costa Mesa CA, Society for Experimental Mechanics, CD-ROM, June 7-11, **2004**.

J.D. Rule, S.R. Wilson, J. S. Moore, "Radical Polymerization Initiated by Bergman Cyclization" *Journal of the American Chemical Society*, 125(43), **2003**, pp. 12992-12993.

E.N. Brown, M.R. Kessler, N.R. Sottos, S.R. White, "In situ poly(urea-formaldehyde) microencapsulation of dicyclopentadiene," *Journal of Microencapsulation*, 20, **2003**, pp. 719-730.

M.R. Kessler, N.R. Sottos, S.R. White, "Self-healing structural composite material". *Composites Part A: Applied Science and Manufacturing*, 34, **2003**, pp. 743-753.

D. Therriault, S.R. White, and J.A. Lewis, "Chaotic mixing in three-dimensional microvascular networks fabricated by direct-write assembly," *Nature Materials*, 2, **2003**, pp. 265-271.

S.R. White, N.R. Sottos, J.S. Moore, P.H. Geubelle, E.N. Brown, J.D. Rule, "Self-healing polymer composites," *Proceedings of the 14th International Conference on Composite Materials (ICCM),* San Diego, CA, Society of Manufacturing Engineering, CD-ROM, July 14-18, **2003**.

E.N. Brown, M.R. Kessler, N.R. Sottos, and S.R. White, "In situ poly(urea-formaldehyde) microencapsulation of dicyclopentadiene," University of Illinois at Urbana-Champaign, TAM Report No. 1014, UILU-ENG-2003-6002, February, **2003**.

J.D. Rule, J.S. Moore, "ROMP reactivity of endo- and exo-dicyclopentadiene," *Macromolecules*, 35, **2002**, pp. 7878-7882.

M.R. Kessler, S.R. White, "Cure kinetics of the ring-opening metathesis polymerization of dicyclopentadiene," *Journal of Polymer Science Part A: Polymer Chemistry*, 40, **2002**, pp. 2373-2383.

INTERACTIONS/TRANSITIONS

Conference Presentations & Seminars

E.N. Brown, N.R. Sottos, S.R. White, "Fatigue crack arrest in a self-healing polymer composite," *Proceedings of SEM Annual Conference on Experimental and Applied Mechanics*, Costa Mesa CA, Society for Experimental Mechanics, June 7-11, 2004.

S.R. White, N.R. Sottos, J.S. Moore, E.N. Brown, A.S. Jones, J. Rule, "Autonomic healing of polymers and composites," *21st International Congress of Theoretical and Applied Mechanics (ICTAM)*, August 15-21, 2004, Warsaw Poland.

S.R. White, N.R. Sottos, K.S. Toohey, "Autonomic healing of polymer coatings," *European Coatings Conference – Smart Coatings III*, June 7-9, 2004, Berlin, Germany.

S.R. White, A.S. Jones, J.D. Rule, and N.R. Sottos, "Self-Healing Polymers," *NanoEurope*, CD ROM, September 13-15, 2005, St. Gallen, Switzerland.

Sottos, N.R., NanoEurope 2005 Conference, *Nanoencapsulation for Multifunctional Polymers*, St. Gallen, Switzerland, Sept. 13-15 (2005).

Sottos, N.R., Motorola Labs, Motorola Nanotechonology Summit, *Nanotechnology for Autonomous Materials Systems*, June 10 (2005).

Toohey, K., White, S.R. and Sottos, N. R., *Self-Healing Polymer Coatings*. SEM Annual Meeting on Experimental and Applied Mechanics, Society for Experimental Mechanics, Portland, OR, June 6-9 (2005).

Sottos, N.R., Princeton University, Department of Mechanical Engineering, *Mechanics of Self-Healing Materials Systems,* April 15 (2005).

Sottos, N.R.,University of California at Riverside, Department of Mechanical Engineering, *Mechanics of Self-Healing Materials Systems,* April 5 (2005).

Moore, J.S. *Self Healing Polymers*, Penn State Colloquium, Penn State, College Station, PA, March 31, 2005.

Moore, J.S. *Advances in Self-Healing Polymers*, ACS Award for Creative Invention (DeSimone), 229th ACS National Meeting, San Diego, CA, March 15, 2005.

Sottos, N.R., University of Illinois at Urbana-Champaign, Beckman Institute Director's Seminar, *Mechanics of Self-Healing Materials Systems*, Feb. 25 (2005).

White, S.R. *Autonomic Healing of Polymers and Composites*, Rheology Research Center Lecture, University of Wisconsin-Madison, Dec. 3, 2004.

S.R. White, N.R. Sottos, B. Blaiszik, M. Keller, A. Rzeszutko, N. Bosscher *Nanocapsules for self-healing composites*, American Society for Composites (ASC) 19th Annual Technical Conference, October 17-20, 2004, Atlanta, GA.

Moore, J.S. *Self-Healing Polymers*, Cherry Emerson Seminar Speaker, Georgia Tech University, Atlanta, GA, September 28, 2004.

White, S.R. *Autonomic healing of polymers and composites*, Keynote address, 21st International Congress of Theoretical and Applied Mechanics, Warsaw, Poland, August 16, 2004.

Moore, J.S. *Self-Healing Polymers*, 228th ACS National Meeting, Division of Business Development and Management, Philadelphia, PA, August 23, 2004.

White, S.R. *Autonomic healing of polymers and composites*, Northrop Grumman Ship Systems. Technology Briefing, The Beckman Institute for Advanced Science and Technology, University of Illinois, July 7, 2004, Urbana, IL.

White, S.R. *Autonomic healing of polymers: status and future plans*, Goodyear Tire and Rubber Company Seminar, Goodyear Research and Development Center, June 14, 2004, Akron, OH.

White, S.R. *Autonomic healing of polymer coatings*, European Coatings Conference – Smart Coatings III, Jun 9, 2004, Berlin, Germany.

Sottos, N.R., Bayer Materials Science, Pittsburg, PA. *Autonomic Healing in Polymers and Composites*, May 27 (2004).

Moore, J.S. *Self-Healing Polymers*, Northwestern Chemistry Colloquia, Northwestern University, Evanston, IL, May 14, 2004.

White, S.R. *Autonomic healing of polymers and composites*, Estee Lauder Corp. Technology Briefing, The Beckman Institute for Advanced Science and Technology, University of Illinois, April 28, 2004, Urbana, IL.

Moore, J.S. *Self-Healing Polymers*, Etter Lecture, University of Minnesota, Minneapolis, MN, February 20, 2004.

Moore, J.S. *Self-healing Polymers*, Departmental Seminar, Queen's University, Kingston, Ontario, January 23, 2004.

D. Therriault, K. Toohey, R. Shepherd, J.A. Lewis, N.R. Sottos, S.R. White *Directed Assembly of 3-D Microvascular Networks for Autonomic Materials*, 2004 Gordon Conference on Composites (poster), Jan. 3-9, 2004, Ventura, CA.

Moore, J.S. *Self-healing Polymers and Other Autonomous Materials Systems*, Breslow Colloquium, Columbia University, New York, NY, December 11, 2003.

Moore, J.S. Self-*Healing Polymers*, Procter and Gamble Graduate Seminar Series, University of North Carolina, Chapel Hill, NC, December 4, 2003.

White, S.R. *Autonomic Healing of Polymers and Composites*, Dana Corporation Technology Briefing, The Beckman Institute for Advanced Science and Technology, University of Illinois, Nov. 18, 2003, Urbana, IL.

White, S.R. *Self-healing composite materials for cryogenic storage tanks*, Air Force Research Lab Cryogenic Composite Tanks Workshop, Oct. 29-30, 2003, Albuquerque, NM.

Moore, J.S. *Self-healing polymers*, IGERT Lecture Series, University of Michigan, Ann Arbor, MI, October 27, 2003.

White, S.R. *Self-healing polymer composites*, Composites at Lake Louise 2003, Oct. 19-23, 2003, Lake Louise, Ontario.

Sottos, N.R. *Self-healing structural polymers and composites*, 40th Society of Engineering Science Technical Meeting, Oct. 13-15, 2003, Ann Arbor, MI.

White, S.R., *Self-Healing Polymers and Composites*, Bio-Inspired Processes for Design, Assembly, and Repair of Electromagnetic and Structural Composites, Georgia Tech University, Atlanta, GA, August 19-20, 2003.

White, S.R., *Multiscale Modeling and Experiments for Design of Self-Healing Structural Composite Materials*, Materials Modeling-The AFOSR MEANS Theme, Boulder, CO, August 6-8. 2003.

White, S.R. *Three-Dimensional Microvascular Networks by Direct-Write Assembly*, Army Research Laboratory Seminar Series, Aberdeen, MD, July 29, 2003.

White, S.R. *Self-Healing Polymer Composites*, 14th International Conference on Composite Materials (ICCM), San Diego, CA, July 14-18 (2003).

White, S.R. *Self-Healing Polymer Composites*, NASA Langley Research Lab Seminar Series, Langley, VA, June 24, 2003.

Sottos, N.R. *Development of Autonomic Materials Systems,* PolynanomerESS: A Matrix for Design to Build Process, an NSF workshop on Nanotechnology, Porto Heli, Greece, June 20 (2003).

White, S.R. *Autonomic Healing of Polymers and Composites*, Army Research Laboratory Seminar Series, Aberdeen, MD, June 17, 2003.

White, S.R. *Self-healing structural polymers and composites*, NASA-Langley Materials Branch Seminar, June 11, 2003, Langley, VA.

Sottos, N.R. *Autonomic Healing of Polymers and Composites*, National Institute of Aerospace (NIA), Morphing Seminar Series, NASA Langley, VA, April 28 (2003).

Sottos, N.R. *Development of Self-Healing Polymers*, The Chicago Microtechnology and Nanotechnology Community International Technology Exchange Workshop, April 24 (2003).

White, S.R. *STTR BMDO/02T-00: Self-healing composite materials for cryogenic storage tanks*, AFRL Contractor's Review Meeting, April 2, 2003, Albuquerque, NM.

Moore, J.S. *Autonomous Materials Systems*, Analytical Chemistry 2002-2003 Colloquium, Texas A&M University, College Station, TX, February 10-12, 2003.

Air Force Lab Collaborations

We partnered with a small business, CU Aerospace (Champaign, IL), for a Phase I STTR managed by AFRL/VSSV on the use of self-healing technology for cryogenic fuel tanks. These tanks are prone to leakage caused by microcracking as they cycle between cryogenic conditions and elevated temperatures. We have also maintain collaborations and technical interactions with AFRL/MLBC on self-healing technology in general, mechanical testing, permeability testing, and multifunctionality.

Transitions

We have worked with several companies through sponsored research agreements to transition self-healing technology into the commercial market. These agreements include Northrop Grumman Ship Systems (coatings, structural composites), CU Aerospace (structural composite tanks), Intel (microelectronics), and Sandia National Laboratories (composite repair).

PATENTS & INVENTIONS

"Microcapillary Networks,"D. Therriault, J. Lewis, and S. White, US Patent Application, September 26, 2003.

"Multifunctional Autonomically Healing Composite Material," S.R. White, N.R. Sottos, P.H. Geubelle, J.S. Moore, S. Sriram, E. Brown, and M. Kessler, US Patent No. 6,518,330, February 11, 2003.

"Catalyzed Reinforced Polymer Composites,"M. Kessler, S.R. White, and B. Myers, US Patent No. 6,750,272, June 15, 2004.

"Wax Particles for Protection of Activators, and Multifunctional Autonomically Healing Composite Materials,"J.S. Moore, J.D. Rule, E.N. Brown, N.R. Sottos and S.R. White, US Patent Application, May 7, 2004.

"Nanoencapsulation Techniques for a Self-healing Polymer," S.R. White, N.R. Sottos, B.J. Blaiszik, UIUC TF06182, filed Nov. 21, 2006.

HONORS/AWARDS

Prof. Scott White was named the Donald Biggar Willett Professor of Engineering (2005-)

Prof. Scott White was named a University Scholar for the UIUC (2005-08)

Prof. Nancy Sottos was named the Donald Biggar Willett Professor of Engineering (2005-)

Prof. Jeff Moore received the UIUC Campus Award for Excellence in Undergraduate Teaching (2004)

Prof. Jeff Moore received the UIUC Liberal Arts & Science Dean's Award for Excellence in Undergraduate Teaching (2004)

Prof. Jeff Moore was named Honorary Lifetime Member Golden Key Honor Society (2004)

Prof. Nancy Sottos received the Hetenyi Award from the Society for Experimental Mechanics (2004).

Prof. Nancy Sottos was named as Editor, *Experimental Mechanics* (2003–).

Prof. Scott White was named a Willett Faculty Scholar (2002-05) for the College of Engineering, University of Illinois.

Prof. Nancy Sottos was named a University Scholar (2002-05) for the University of Illinois.

Prof. Nancy Sottos was named to the Editorial Board of Composite Science and Technology (2002–).

Graduate student Joe Rule holds a Hertz Foundation Fellowship (2001-05).

Graduate student Daniel Therriault holds a Center for Nanoscience and Technology Fellowship (2002).

Prof. Jeffrey Moore was named an AAAS Fellow (2003).

Graduate student Joe Rule received the Procter & Gamble Graduate Research Award (April 2004).

Graduate student Joe Rule received the Seemon Pines Award (Best Presentation at the Allerton Conference, October 2003).

Prof. Scott White received the Army Research Lab Faculty Fellowship (2003).